

A Short Time-series of Dust and Ice Isotopic  
Composition (Sr, Nd and Hf) from the Dye-3 Ice  
Core, Greenland.

Maarten Lupker

December 2007

With Supervision By:

**Dr. Sarah M. Aciego**

**Prof. Bernard Bourdon**

*Institute of Isotope Geochemistry and Mineral Resources - ETH Zurich*

## Abstract

Determining the source and pathway of atmospheric dust remains a difficult problem. This work presents geochemical techniques for separating and measuring radiogenic isotopes found in dust within ice cores, and the resulting record from using these new techniques. A four step separation scheme was set up using ion exchange columns for separation of the low concentration elements and the method was validated using the certified BCR-2 rock standard. The measured ice core record is a short, high resolution (yearly to seasonal) time series of Sr and Nd isotopic composition of both dust and ice from the  $\sim 128\text{m}$  to  $132\text{m}$  section of the Dye-3 (88) ice core in Greenland. Hf isotopic composition was also measured for 3 of the dust samples as a complementary tracer of dust origin, the first direct measurement of Hf in paleo-atmospheric dust. Measured Nd and Sr isotopic composition of the dust compared to literature potential source area (PSA) data ( $<5\mu\text{m}$  size fraction) shows variability of the potential source area on short time scales. Asia is identified as one potential source to the Greenland dust load; the primary contribution varies between the Taklimakan desert, Gobi desert and the Ordos Plateau. Another dust source mixing with the Asian dust is invoked to explain the variability in the isotopic composition of the ice core dust, but the source area has not been identified because of the lack of adequate sampling of PSAs. The radiogenic isotopes within the ice fraction is found to be of oceanic origin; the  $^{87}\text{Sr}/^{86}\text{Sr}$  values, close to seawater, and  $\epsilon_{\text{Nd}}$  variations are decoupled from dust composition. Ice isotopic composition is thought to be derived from sea salts or sea ice brine and that measurement of Sr and Nd could constitute a valuable tool for climate reconstructions.

**Keywords:** dust; ice core; Greenland; Dye-3; Sr isotopes; Nd isotopes; Hf isotopes; potential source area

## Résumé

La détermination des sources et du transport des aerosols minéraux dans l'atmosphère reste un problème difficile. Ce travail rend compte des techniques géochimiques de séparation et de mesures d'isotopes radiogéniques présents dans les poussières minérales des carottes de glace ainsi que des résultats acquis grâce à ces nouvelles techniques. Un processus de séparation en 4 étapes utilisant des résines échangeuses d'ions a été développé et la méthode validée en utilisant le standard de roche certifié BCR-2. Les mesures effectuées montrent un court enregistrement à haute résolution (annuelle à saisonnière) de la composition isotopique du strontium et du néodyme de la fraction minérale et de la glace sur une section (~128m à 132m) de la carotte de glace Dye-3 (88) prélevée au Groenland. La composition isotopique du hafnium a aussi été mesurée pour trois échantillons de poussière comme traceur d'origine complémentaire, ce qui constitue les premières mesures directes de Hf sur des poussières paleo-atmosphériques. La comparaison des mesures isotopiques de la poussière prélevée avec les compositions des régions sources potentielles trouvées dans la littérature (fraction de taille inférieure à  $5\mu\text{m}$ ) montrent des variations de source à petits intervalles de temps. L'Asie est identifiée comme ayant contribué à la charge de poussières du Groenland avec une contribution majeure variant entre les déserts du Taklimakan et de Gobi d'une part et du Plateau d'Ordos d'autre part. Une autre source est nécessaire pour expliquer la variabilité de la composition isotopique de la poussière mais cette région n'a pu être identifiée en raison du manque d'échantillons adéquats. Les isotopes radiogéniques contenus dans la glace montrent une origine marine;  $^{87}\text{Sr}/^{86}\text{Sr}$ , proche des valeurs océaniques et les variations d' $\epsilon_{\text{Nd}}$  sont découplées de la composition de la poussière. La composition isotopique de la glace est supposée provenir d'aerosols marins ou de sels précipités à la surface de la glace de mer et la mesure du Sr et du Nd pourrait être de précieux outils pour des reconstructions climatiques à venir.

**Keywords:** poussières; carotte de glace; Groenland; Dye-3; isotopes du Sr; isotopes du Nd; isotopes du Hf; sources potentielles.

## Acknowledgments

I wanted to specially thank Sarah M. Aciego, as my supervisor and as a friend for all the time she spend introducing me to this exciting topic of ice core studies, for transmitting me her scientific rigor and enthusiasm but also for the good moments we had during those 5 month.

I wanted also to thank Bernard Bourdon for offering me a place in his group as a master student and for giving me at my disposal the means without which this work wouldn't have been possible.

I also have a though for the whole IGMR group for their help and friendly attitude. Specially Felix Oberli for his numerous advices concerning the methods and Jörg Rickli for all the fruitful discussions we had, his help for the Hf measurements set up and also just for his good mood...

Thanks also to Jakob Schwander and Thomas Stocker for providing us with the ice core and to Stefano Bernasconi for the oxygen measurements.

# Contents

<b>1</b>	<b>Introduction</b>	<b>7</b>
1.1	Ice as a climatic archive . . . . .	7
1.2	Dust in polar ice . . . . .	9
1.2.1	Dust concentration and composition . . . . .	9
1.2.2	Potential source areas (PSAs) of dust . . . . .	9
1.2.3	Tracing dust sources . . . . .	10
1.2.4	Origin of Greenland dust . . . . .	12
1.3	Objectives and Samples . . . . .	15
<b>2</b>	<b>Methods</b>	<b>16</b>
2.1	Measurement techniques . . . . .	16
2.1.1	Inductively Coupled Plasma Quadrupole Mass Spectrometer - ICPQMS . . . . .	16
2.1.2	Multi-Collector Inductively Coupled Plasma Mass Spec- trometer - MC-ICPMS . . . . .	18
2.1.3	Thermal Ionization Mass Spectrometer - TIMS . . . . .	19
2.2	Analytical procedures . . . . .	20
2.2.1	Reagents: . . . . .	21
2.2.2	Cleaning procedures: . . . . .	21
2.2.3	Clean lab facilities: . . . . .	22
2.3	Elemental separation scheme . . . . .	22
2.3.1	Principles of ion exchange chromatography . . . . .	22
2.3.2	A four step separation scheme . . . . .	23
2.4	Isotopic systems . . . . .	26
2.4.1	Definitions and methods . . . . .	26
2.4.2	Strontium - Sr . . . . .	29
2.4.3	Neodymium - Nd . . . . .	32
2.4.4	Hafnium - Hf . . . . .	34
2.5	Ice processing . . . . .	37
2.5.1	Decontamination and melting . . . . .	37
2.5.2	Filtering . . . . .	38
2.5.3	Sample dissolution . . . . .	39
<b>3</b>	<b>Results</b>	<b>40</b>
3.1	Rock standards . . . . .	40
3.1.1	Strontium - Sr . . . . .	40
3.1.2	Neodymium - Nd . . . . .	41
3.1.3	Hafnium - Hf . . . . .	42
3.2	Ice and dust fractions . . . . .	44

<b>4 Discussion</b>	<b>48</b>
4.1 Dust provenance . . . . .	48
4.2 Isotopic composition of the ice . . . . .	51
<b>5 Conclusion</b>	<b>54</b>
<b>A Lead: methods, results and pitfalls</b>	<b>II</b>
<b>B Column elution procedures</b>	<b>VI</b>
<b>C Measuring U-Series Isotopes in Polar Ice</b>	<b>XIV</b>

## List of Figures

1	Greenland ice sheet and major ice core drilling sites. . . . .	8
2	Global distribution of dust source from TOMS instrument . . . . .	10
3	Strontium and neodymium isotopic ratios of northern-hemisphere PSAs. . . . .	12
4	Localization of PSA samples from literature data. . . . .	13
5	Strontium and neodymium isotopic ratios of northern-hemisphere PSAs and dust fraction of Greenland ice cores. . . . .	14
6	Schematic diagram of an ICP plasma torch, from NuInstruments (1998). . . . .	17
7	Schematic diagram of the Nu Plasma MC-ICPMS, adapted from Rehkämper <i>et al.</i> (2001). . . . .	18
8	Single and double filaments for TIMS ion source, from ThermoFinnigan (2002). . . . .	20
9	Elemental separation scheme. . . . .	24
10	Sr NBS987 runs . . . . .	31
11	Nd JNdi-1 runs . . . . .	34
12	Hf JMC475 runs . . . . .	37
13	Sr BCR-2 measurements . . . . .	40
14	Nd BCR-2 measurements . . . . .	41
15	Hf BCR-2 measurements . . . . .	42
16	Strontium and neodymium composition of Dye-3 dust and ice fractions as a function of depth. . . . .	47
17	Neodymium and hafnium composition of Dye-3 dust and ice compared to literature data - (a) dust and ice isotopic composition - (b) details of ice isotopic composition. . . . .	49
18	Neodymium and hafnium composition of Dye-3 dust and ice. Asian dust member and Nd-Hf correlation of modern aeolian dust are from Pettke <i>et al.</i> (2002). . . . .	51
19	$\beta$ factor calculated from NBS981 measurements. . . . .	IV
20	Elution curve obtained from the Truspec column using the BCR-2 rock standard. . . . .	VII
21	Elution curve obtained from the Srspec column using the BCR-2 rock standard. . . . .	IX
22	Earlier elution curve obtained from the Lnspec column using the BCR-2 rock standard. This column was further calibrated and final Hf yields were over 96 %. . . . .	XI
23	Elution curve obtained from the Lnspec REEs separation column using the BCR-2 rock standard. . . . .	XIII

# 1 Introduction

## 1.1 Ice as a climatic archive

Old ice in polar and high altitude regions is one of the few direct records of past climate. Precipitation falls as snow and the layers of snowfall (seasonal, annual, etc) are compressed and thinned, gradually transforming from snow to firn to ice. The chemical composition of the precipitation, solid particles that are deposited with the snow, and the air trapped within the snowmass will remain unchanged through this transformation if the ice remains unexposed after initial deposition. The length of time recorded in these ice layers is a function of the ice thickness, flow dynamics, and amount of time that the accumulation area has remained undisturbed. For these reasons, ice cores drilled from ice flow divides can record 100-700 ka of precipitation and atmospheric conditions.

The early success of initiatives taken during the 1957-1958 International Geophysical Year, with the U.S. Antarctic field campaign drilling at Byrd Station and Little America V, resulted in a high level of interest in recovering ice cores. During the past decades efforts have been made recovering ice cores from Greenland, Antarctica and high mountain glaciers despite difficult access and logistical complications. The Greenland Ice Sheet Project (GISP) was founded in 1970 by research groups from the United States, Denmark and Switzerland for a multidisciplinary study of ice sheets. The primary aims were mapping the thickness and subsurface topography of the ice sheet and drilling several cores to bedrock (Langway *et al.*, 1985). Early field work focused on finding the optimum site for a deep core, with correspondingly old ice, as well as at the development of technical solutions. The Dye-3 core commenced in the summer 1981 at Dye-3 site and, after three seasons of drilling, bedrock was reached at 2037m (Dansgaard *et al.*, 1982). A U.S. follow up program, GISP2, drilled near to the summit of the Greenland ice sheet and reached bedrock in 1993 after five years and 3054m of ice. In parallel, the european GRenland Ice-core Project (GRIP) reached bedrock in 1992 in the same summit area and recovered a 3029m ice core (Grootes *et al.*, 1993). The locations of these ice core sites are noted in Figure 1.

The valuable information retrieved from ice cores allows us to interpret past and present climate as well as make predictions about future climate change. Ice composition, specifically oxygen and hydrogen isotopes, yield information about temperature conditions during deposition, ice volume and the hydrological cycle (e.g. Petit *et al.*, 1999). The study of air bubbles trapped in the ice is an indicator of past atmospheric composition, for instance, the greenhouse gases CO<sup>2</sup> and CH<sup>4</sup> (e.g. Barnola *et al.* (1987) and Chappelaz *et al.* (1990)). Determining the age

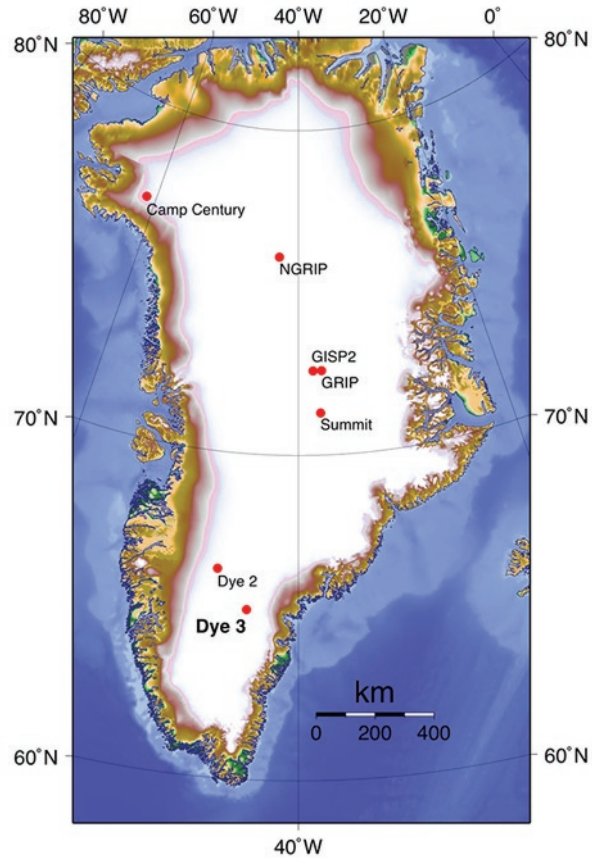


Figure 1: Greenland ice sheet and major ice core drilling sites.

of the ice layers relies on age markers such as (1) the summer insolation record, as indicated in the  $O_2$  and  $O_2/N_2$  gas records, (2) cosmic ray produced  $^{10}Be$  record (e.g. Raisbeck *et al.*, 1987), and (3) volcanic ash layers (e.g. Clausen *et al.*, 1997). Among the different indicators of past climate in ice cores, the changes in insoluble airborne mineral aerosols, hereafter termed dust, records differences in atmospheric conditions through time. Mineral dust is a major component of the overall atmospheric aerosol loading and an established climatic forcing factor (IPCC AR4, 2007). Dust can also affect oceanic productivity by supplying nutrient to the marine environment, thereby affecting the global carbon cycle (Martin, 1991).

## 1.2 Dust in polar ice

### 1.2.1 Dust concentration and composition

Dust content of ice-cores integrates information about the processes that form, transport and deposit dust. The dust content of Greenland ice core samples show seasonal variations and is strongly correlated with the  $\delta^{18}\text{O}$  record on short time scales (Hamilton & Langway, 1967). On longer time scales, dust concentration correlates with temperature and is one to two orders of magnitude higher during glacial periods than in interglacial (ranging from tens of  $\mu\text{g}/\text{kg}$  ice to a few thousand) (Hammer *et al.* (1985); Ram & Koenig (1997)). A possible explanation for this observation is a "slower" water cycle and stronger atmospheric circulation that could account for a more efficient dust production and transport during the cold periods (Xiao *et al.*, 1996).

Size distributions of Greenland dust have a log-normal distribution around 1-2 $\mu\text{m}$  (Steffensen (1997) and Ruth *et al.* (2003)) consistent with long range transport models (Schulz *et al.*, 1998) and other Northern Hemisphere dust deposits in snow (Zdanowicz *et al.* (2006) and references therein). Carbonates and evaporites have been found in African dust (Chester & Johnson (1971); Prospero *et al.* (1981); Schutz & Seibert (1987)) as well as in Asian dust (Schi *et al.* (2005) and Sullivan *et al.* (2006) and references therein). But, little is known about their conservation during transport and deposition even though these minerals are found in Greenland dust (Biscaye *et al.* (1997); Svensson *et al.* (2000)). The silicate fraction of ice core dust is mainly composed of clay assemblages (chlorite, illite, smectite, kaolinite), quartz and feldspars (Biscaye *et al.* (1997); Svensson *et al.* (2000); Bory *et al.* (2003b)).

### 1.2.2 Potential source areas (PSAs) of dust

The main sources of atmospheric dust are situated in arid areas and the deserts where sand dunes, dry soils, lack of vegetation or lake beds are concentrated in available dust material. These regions are immediately recognizable in fig.2, a global distribution map of current dust sources. Most of these areas are situated at the latitude of the tropics where the descending branch of the Hadley circulation accounts for dry air, e.g. the Sahara, Arabia and North American deserts. Dust sources situated at higher latitudes are associated with continentality and orography, which are responsible for low precipitation, e.g. the Northern Tibet and Inner Mongolian deserts.

Total annual and global dust emissions have been estimated from dust model studies to range between 1000 Tg/yr and 2000 Tg/yr with North Africa accounting for more than half of this budget ( $\sim 50\%$ ) followed by Arabia ( $\sim 25\%$ ) and Asia

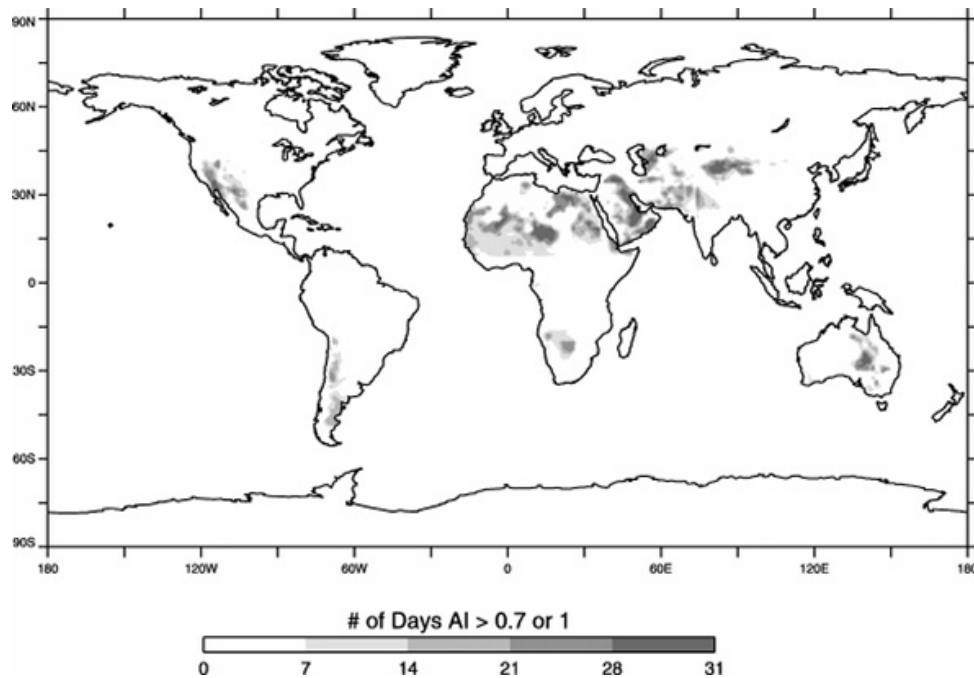


Figure 2: Global distribution of dust source from TOMS instrument  
Expressed in number of days per month with an Aerosol Index (AI) higher than 1 in the dust belt and 0.7 elsewhere using those month which best illustrate the configuration of specific dust sources, from Prospero *et al.* (2002).

(~15%). Contributions of North America, South America and Australia vary from study to study but are overall low (Tanaka & Chiba (2006) and references therein).

### 1.2.3 Tracing dust sources

#### Size fractions and mineralogy:

In order to determine the dusts' origin, mineralogical and physical arguments have often been used. Grain size distributions have been used as characteristics of source areas (e.g. Sarin *et al.*, 1981), but these have been found to be affected and biased by variable transport conditions such as wind speed and travel distance (Rea, 1994).

Mineralogical composition and especially clay mineralogy has proven to be a good tool for provenance studies. Clay minerals are relatively well conserved during transport which is of first importance. Clay assemblages are also a function of climate, through varying weathering processes, which is then in turn a "fingerprint" of some source areas. For instance, Biscaye (1965) proposed to use the kaolinite to chlorite ratio (K/C) as an indicator of latitude of the

sediments, kaolinite being preferential formed during chemical weathering in warm moist environments, typical of lower latitudes and chlorite, mostly from primary origin and preserved during physical weathering occurring mostly in high latitudes.

### **Isotopic fingerprints:**

One powerful tool for determining dust origin is the isotopic composition of the dust. This tracer is considered a robust estimator of source because the radiogenic isotopic composition should not be fractionated during transport and shows variability between source regions. Strontium isotopes have been demonstrated to indicate the dust sources for Hawaiian dust deposits (Dymond *et al.*, 1974). More recently, other isotopic systems have been introduced to better constrain dust origin. Neodymium isotopes have been used extensively to resolve sources areas with very similar Sr ratios and the combination of Sr and Nd ratios has been found to be an excellent "fingerprint" in most cases (Grousset & Biscaye (2005) and references therein). Lead isotopes have also been used to distinguish sources (Jones *et al.* (2000); Biscaye *et al.* (1997)), although Pb isotopic composition often bears a strong anthropogenic signal that may complicate the determination of "natural" lead, *i.e.* that is derived from rock weathering and not from pollution. Pettke *et al.* (2002) have also applied hafnium isotopes to dust provenance in Asia indicating that Hf is a potential tracer. But, little information is available on the Hf isotopic composition of Potential Source Area samples (PSAs).

The primary complication in applying isotopic signatures as direct source "fingerprints" comes in determining the composition of the *transportable* source area dust. Studies have shown that Sr isotopic ratios are size fraction dependent (Dasch, 1969) and this has been verified on aerosols (Kanayama *et al.*, 2005) and Asian PSA samples (Chen *et al.*, 2007). Nd isotopes are less sensitive to size fraction in loess and desert sands (Yokoo *et al.* (2004); Rao *et al.* (2006); Chen *et al.* (2007)) even-though size dependent variations have been found in other studies (Derry & France-Lanord, 1996). The constrains imposed by the long distances transport thus requires looking at consistent size fractions between source and sink dust, *i.e.* only the smaller size fraction ( $< 5\mu m$ ) of PSA samples can be used.

Weathering is also known to affect Sr isotopic ratios: the leaching of carbonates with low  $^{87}Sr/^{86}Sr$  ratio, induces an increase of the bulk sample's  $^{87}Sr/^{86}Sr$  ratio with weathering (e.g. Gallet *et al.*, 1996). Nd is not so abundant as Sr in carbonates and Nd isotopes have not been found to be affected by carbonate leaching (Jones *et al.*, 1994). To remove this bias, carbonate fraction of

PSA samples of the northern hemisphere are commonly removed by leaching with acetic acid (Biscaye *et al.* (1997); Kanayama *et al.* (2002); Chen *et al.* (2007)) although exact procedures differ from study to study. These precautions enable differentiation of PSAs according by isotopic composition of the silicate fraction.

These minimum requirements of long-range transport, small size fraction and carbonate leaching, results in a bias toward the Asian datasets and large source areas such as African and Arabia are not represented by the data. A compilation of the existing Sr and Nd data for PSA samples is shown in Figure 3, indicating the distinct variability in North America and Asian source composition. The locations of these PSA samples are mapped in Figure 4, which also further illustrates the limited number of samples that have been collected and analyzed in other Northern Hemisphere arid locations.

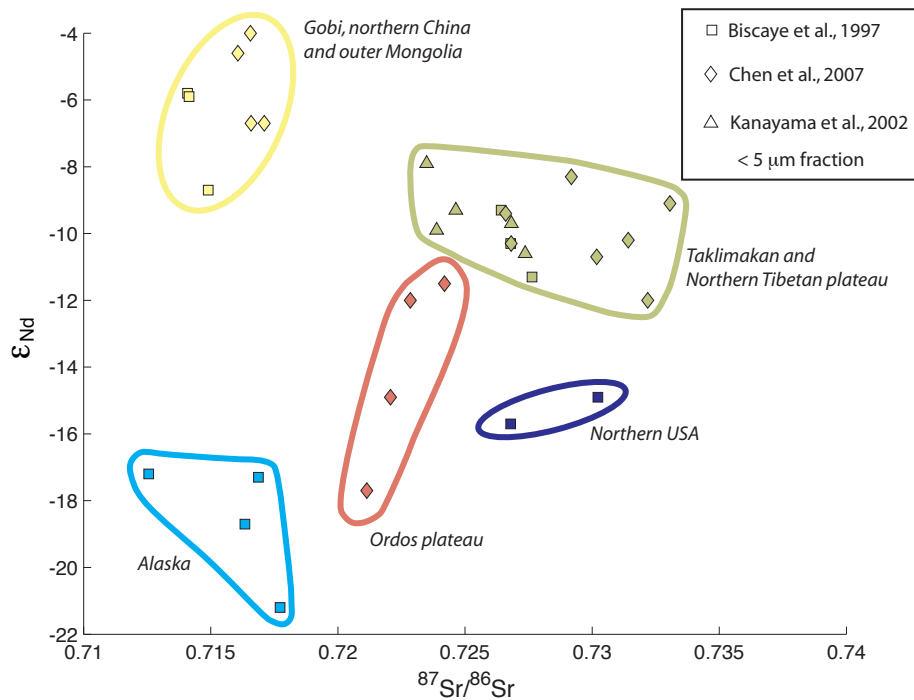


Figure 3: Strontium and neodymium isotopic ratios of northern-hemisphere PSAs. Literature data of carbonate free,  $< 5\mu\text{m}$  fractions. The  $^{143}/^{144}$  neodymium ratio is expressed in epsilon units (c.f. 5-p.32).

#### 1.2.4 Origin of Greenland dust

Several studies have purported to have determined the dust origin in Greenland ice cores. The combination of mineralogical studies (K/C ratios) and isotopic

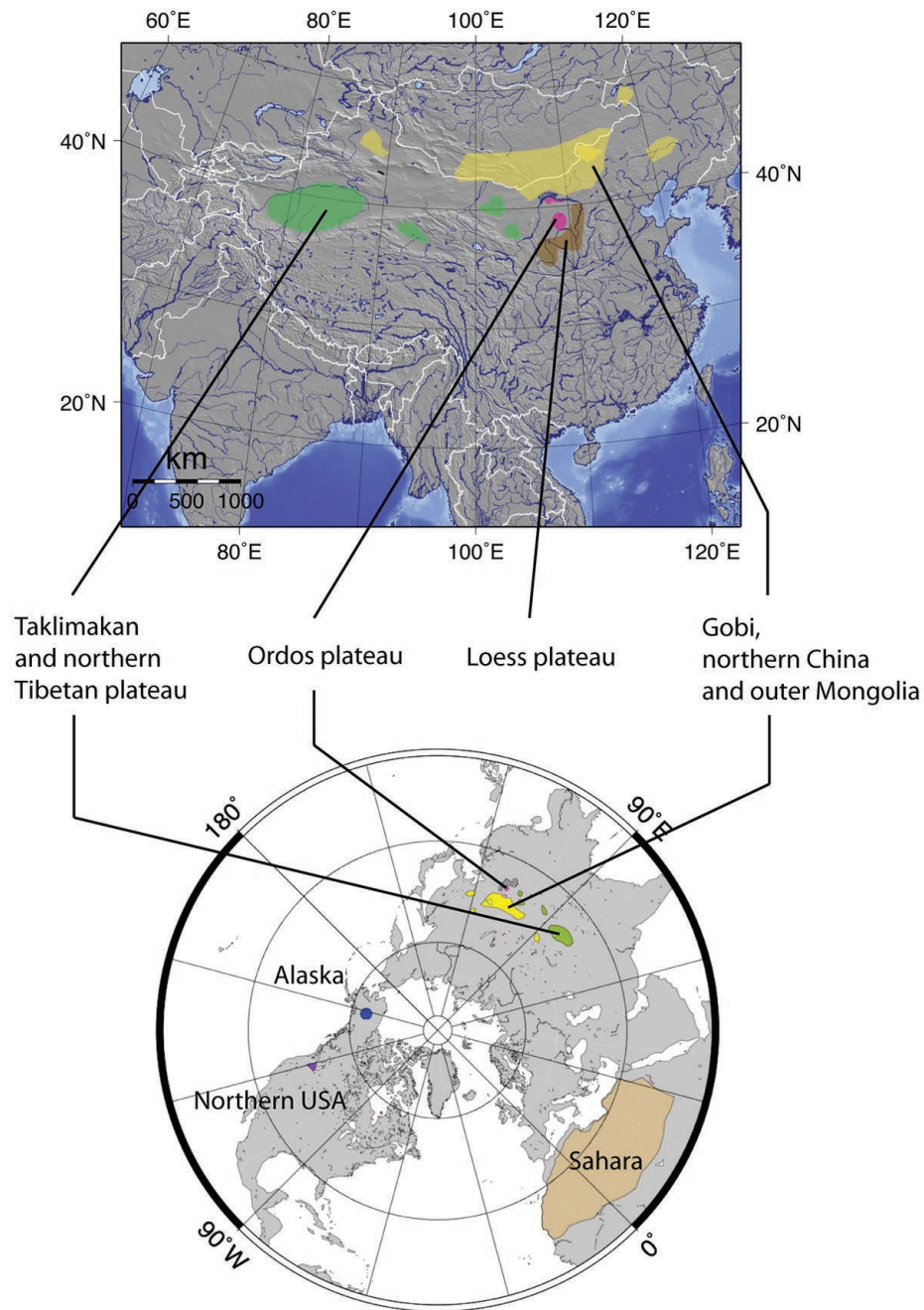


Figure 4: Localization of PSA samples from literature data.

measurements (Sr/Nd/Pb) on the dust silicate fraction extracted from the GISP2 and GRIP ice cores suggested that Asia was the main source of Greenland dust at summit during glacial periods (Biscaye *et al.* (1997); Svensson *et al.* (2000)

and Burton *et al.* (2007)). Based on similar arguments, an Asian origin was also found in Holocene ice core sections across the interior of the Greenland ice sheet (Bory *et al.*, 2003b) and in contemporaneous snow pits from the NGRIP site (Bory *et al.* (2002) and Bory *et al.* (2003a)) (c.f. fig. 5).

Due to analytical limitations, dust isotopic measurements and mineralogy were carried out on long core sections integrating several years to decades of dust deposition history making the differentiation of source regions contributing to the overall dust signal even more difficult. By comparing isotopic characteristics of extracted dust from ice cores and different asian source areas, previous workers have suggested that the Gobi and Taklimakan desert are the best candidates for the dust load in Greenland. A systematic shift towards less radiogenic  $87^{Sr}/86^{Sr}$  of the dust in Greenland compared to PSA values is attributed to mixing with circum pacific volcanic aerosols that may contribute up to 25 % of the dust load (Biscaye *et al.*, 1997). High resolution (2 month to annual) snowpit dust samples, allowed Bory *et al.* (2002) and Bory *et al.* (2003a) to detect a seasonal variability in dust origin, which the authors attributed to a dominant Taklimakan source in spring and and Inner Mongolian source in autumn.

The contribution of other PSA mineral dust in Greenland has not yet been shown. The possibility of a Saharan contribution was rejected by Biscaye *et al.* (1997) based on lead isotopes but, to our knowledge, no Sr and Nd isotopic data is available for this region. And, Northern America (including Canada) is also a potential candidate for exporting dust to Greenland. Donarummo *et al.* (2003) proposed that the central U.S. plains are important dust sources for Greenland during severe droughts and identified a possible event. Palynological evidence (plant pollen) also points toward North America as a potential source area (Rousseau *et al.*, 2006).

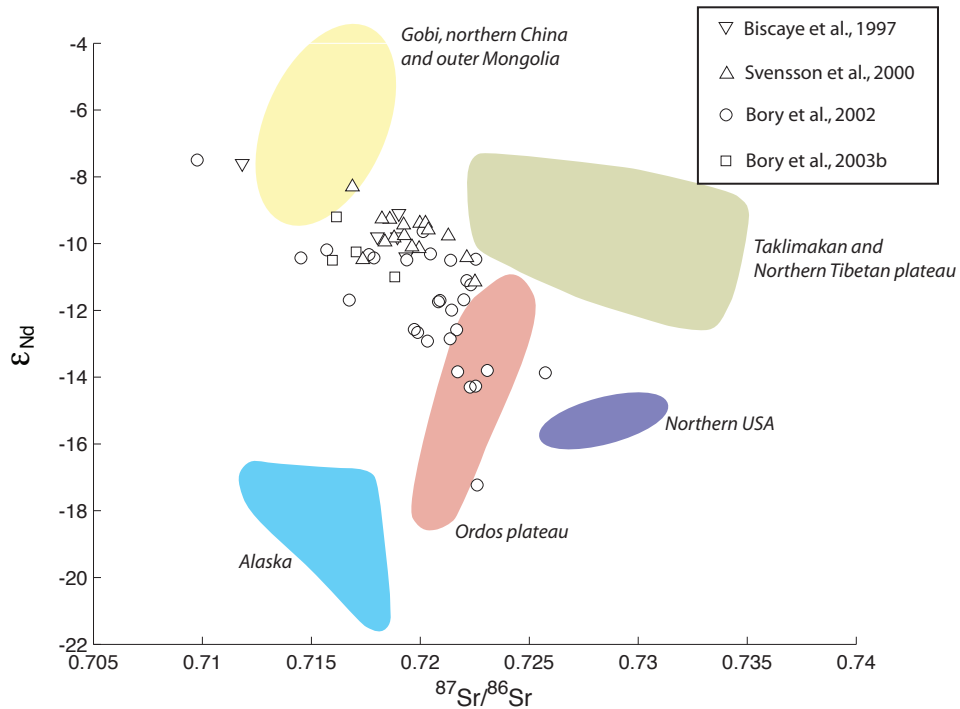


Figure 5: Strontium and neodymium isotopic ratios of northern-hemisphere PSAs and dust fraction of Greenland ice cores.

Carbonate free samples. Data from coastal ice core sites has been omitted.

### 1.3 Objectives and Samples

The short time scale variability of dust sources transported to Greenland found in snow pits shows the importance of high resolution dust studies in order to fully capture atmospheric and source area processes. In this work we try to investigate the feasibility of yearly to seasonal dust isotopic analysis on a Greenland ice core. If successful, higher resolution analyses could be a valuable tool for further climate reconstructions if extended to other ice core sections. This high resolution study could reveal processes that may not have been detected by longer time averaged samples used in other studies and possibly refine source areas contributions to Greenland dust. Hafnium isotopes are also investigated as a potential complementary isotopic tracer for dust origin that may help in PSA discrimination.

In addition to dust analysis, we also focused on the isotopic composition of the dust free ice fraction and the possible relation to transport mechanisms and atmospheric conditions at the time of deposition, which are not yet fully understood.

The samples used in this work are part of the 200m deep ice core drilled at the Dye-3 site (65°11'N, 43°49'W) in 1988 (c.f. figure 1) on the Greenland ice sheet. The mean annual temperature recorded at Dye-3 is -19.6°C with a yearly accumulation of 0.55m ice equivalent. This ice core was drilled c.a. 600m to the west of the station and 150m apart from the 1979-81 Dye-3 deep core (Sigg (1990); Vinther *et al.* (2006)). The high accumulation rate of the Dye-3 site is responsible for low dust concentrations in the ice core of 0.1 to 0.2 mg/kg for Holocene ice (Hammer *et al.*, 1985). The samples were 10.2 cm diameter ice core sections from 129m to 133m depth from which 1m (131) was missing. Samples were provided by the University of Bern, Switzerland (J. Schwander and T. Stocker).

## 2 Methods

### 2.1 Measurement techniques

The isotopic and elemental composition of inorganic samples is commonly investigated using mass spectrometry. The Mass Spectrometer (MS) instruments are designed to separate and analyze ions according to the mass to charge ratio.

MSs are divided in three main parts:

- the ion source, where the atoms of the sample are ionized,
- the mass analyzer, where the ions are separated depending on their mass and their charge,
- the detector, where the ion beams are transformed into a signal that enables the determination of the number of ions produced.

During this study, three different types of mass spectrometers were used, and they will briefly be introduced in the following sections.

#### 2.1.1 Inductively Coupled Plasma Quadrupole Mass Spectrometer - ICPQMS

The ICPQMS used at the IGMR-ETHZ lab is a Perkin-Elmer Elan <sup>®</sup> DRC-e.

**Sample introduction and ion source:** The samples are introduced as liquid solutions. A peristaltic pump draws liquid through the nebulizer and into the spray chamber. Interaction of an argon gas flow with the solution within the nebulizer breaks the solution in small droplets (aerosols) and directs the vapor into the spray chamber. The tilted spray chamber design removes the largest aerosols from the vapor, allowing the finest fraction to pass into the torch region. The remaining aerosols are introduced to the plasma by the sample injector and ionized.

The ionization takes place in a high temperature (6000-7000K) argon plasma in a quartz torch (cf. figure 6). This plasma is maintained through an alternating current circulating around the torch in a copper coil inducing an intense electromagnetic field at the end of the torch. A high voltage spark induces the ionization of argon, and the generated free electrons are kept in the magnetic field and initiate the ionization of the surrounding particles.

**Interface:** The ionization process takes place at ambient pressure, while the ion beam is measured at lower pressure (typically  $10^{-6}$  Torr), therefore the beam is directed into and through the machine at progressively lower pressures. The

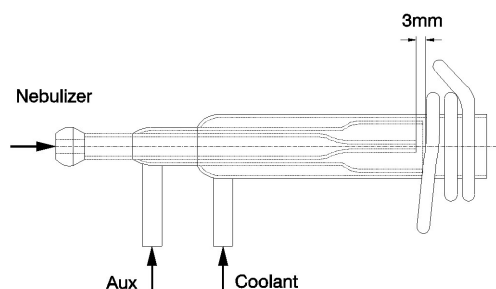


Figure 6: Schematic diagram of an ICP plasma torch, from NuInstruments (1998).

initial transfer is through an intermediary of a set of cones (sampler and skimmer cone) with small orifices. Due to the pressure drop after each cone, the plasma undergoes rapid expansion and only a fraction of the ions, with a uniform kinetic energy distribution, is transferred to the instrument.

**Lenses and mass analyzer:** The ion beam is first accelerated by a high voltage potential difference. Then, in order to transfer the maximum amount of analyte ions through the instrument and to minimize the interaction with other matrix ions that tend to defocus the beam (space charge effects), the beam goes through a set of lenses. These electrostatically controlled lenses ensure that the beam is well focused and steered before entering the mass analyzer.

In a quadrupole mass spectrometer, four identical rods aligned along the incoming beam separate the ions based on the mass to charge ratio. By applying a direct current on one pair of rods and a varying on the other pair it is possible to select and steer the chosen ions to the detector and eject the other ions.

**Detectors:** The quadrupole mass spectrometer is equipped with a single detector, based on a channel electron multiplier. The ions emerging from the quadrupole are impacting a semiconductor cone and are converted to electrons. The electrons produce secondary electrons by further impaction on the detector. The signal generated is a discrete pulse that is generated from all the secondary electrons and is detected by a fast amplifier. By filtering the incoming ion beam and using both discrete and analog counting modes, this system is able to cover a large dynamic range that allow the detection of various beam sizes.

Application:The fast start-up, versatility and ability to analyze numerous elements in a short amount of time make the quadrupole particularly well suited to analysis of large numbers of solutions with multiple element analyses per solution. The detectors, covering a large concentration range, are also well suited to situations where the concentration of the different analytes is not well known and

varies from sample to sample.

During this study the ICPQMS was mainly used for column calibrations and monitoring blanks. For these tasks where the isotopic ratios were not necessary and the amount of the analyte high, the quadrupole was used to determine the relative elemental abundances.

### 2.1.2 Multi-Collector Inductively Coupled Plasma Mass Spectrometer - MC-ICPMS

The MC-ICPMS in operation at the IGMR and used here are Nu Instruments® plasma mass spectrometers.

The operation of the sample introduction system, the ion source, the interface and lenses of the Nu is close to the one of the quadrupole, the major differences are found in the mass analyzer system and the detectors (cf. figure 7).

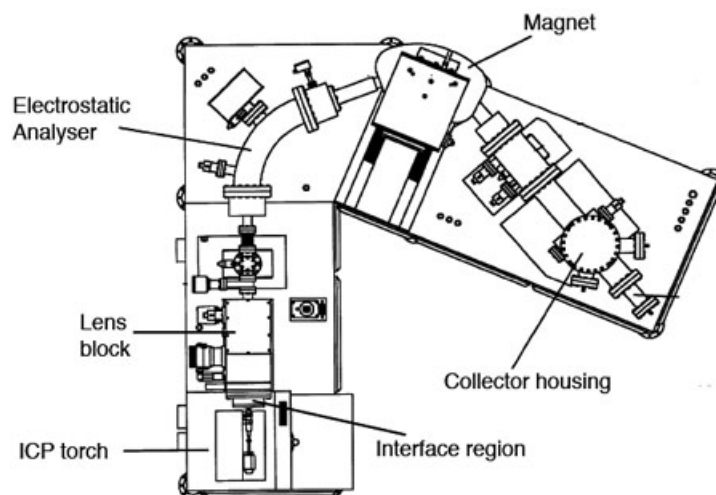


Figure 7: Schematic diagram of the Nu Plasma MC-ICPMS, adapted from Rehkämper *et al.* (2001).

**Mass analyzer:** In these instruments, the separation of the different analytes is achieved using a double focusing magnetic sector. The ions are extracted from the plasma, accelerated and directed into the mass analyzer. First, the beam is focused through an electrostatic analyzer (dispersive in ion energy only) that compensates for the large energy spread of the ions produced in the plasma. Then the ions are directed through a magnetic field that focuses both the ion energy and mass. The electrostatic analyzer is set to exactly compensate the

displacement produced by the magnet.

**Detectors:** After passing through the mass analyzer, the ion beam is split into different beams, one for each mass to charge ratio. For the beam intensities used during this study ( $> 20$  mV), the ions were directed into Faraday cups, *i.e.* a metal electrode that monitors the current induced by the the charged ion beam and that is proportional to the abundance of the analyte measured. This current is converted to a voltage through a  $10^{11}\Omega$  resistance.

The Nu Instruments are equipped with an array of 12 faraday cups, which allows the continuous and simultaneous monitoring of up to twelve ion beams, increasing accuracy of measurements. The faraday cups are fixed and the peak alignment (directing the right ion beam into the right cup) is through a set of lenses between the magnet and the collector box.

For more information about MC-ICPMS refer to Rehkämper *et al.* (2001), Thomas (2001) or the Nu plasma manual (NuInstruments, 1998).

Application: During this study, the Hafnium isotopic measurements were carried out on the Nu instrument. The high sensitivity of the MC-ICPMSs makes them less suited to bulk solution analysis because the range of concentrations is large in natural samples and may damage the cups. Because of the low abundances and high ionization potential of Hf, a high yield ion source is needed, which is the case of an ICPMS. Furthermore the sample preparation prior to the measurement is easy and some previous experience on low concentration Hf measurements with the Nu plasma was available at the IGMR - ETH Zurich (J.D. Rickli).

### 2.1.3 Thermal Ionization Mass Spectrometer - TIMS

For this study, a Thermo Finnigan TRITON® TIMS was used.

TIMS machines mainly differ from previously discussed mass spectrometers in the ion source.

**Sample loading and ion source:** In a TIMS, the sample is loaded on a filament that is installed on a rotating turret and loaded into the machine. By heating the filament with a current, the sample is evaporated off the filament and subsequently ionized.

The alternate ion source has several advantages over the plasma source if the element of interest has low enough ionization potential. First, the ion source is already at low pressure ( $\sim 10^8$  Torr) so the transfer of the ions from the source to the mass analyzer is more efficient. Second, the full control on the heating

temperatures yields a better stability of the ion beam, and permits a selective ionization of different species that have different evaporation/ionization temperatures.

Different kinds of filament systems can be used. On single filament assemblies, evaporation and ionization occur on the same filament whereas on double filaments, the sample is evaporated off one filament and then ionized by a second filament that can have a different temperature (cf. figure 8). Depending on the analyzed element, the sample can be loaded with activator solutions that enhances ionization, such as tantalum (Ta) or silica gel, by decreasing the work function of the electrons on the filament (the energy needed to extract an electron from a solid).

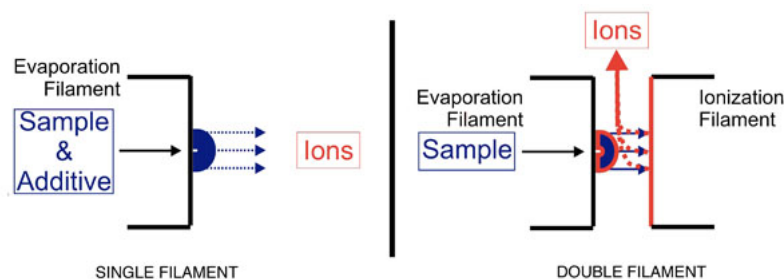


Figure 8: Single and double filaments for TIMS ion source, from ThermoFinnigan (2002).

For more information about the TRITON refer to ThermoFinnigan (2002).

Application: The TRITON was used for the isotopic analysis of strontium, neodymium and lead. While the loading of the samples is time consuming and requires some practice, the stability and precision of the measurements enables the measurement of very small samples with a high reproducibility.

Due to the low temperatures (1000-1800°C) achieved in the ion source, this technique is only suited to elements with a relatively low ionization potential.

## 2.2 Analytical procedures

The small samples analyzed for this work require ultra-clean procedures; both in chemical purity and vials that contact the sample material.

### 2.2.1 Reagents:

- Water: Two types of water were used. For regular cleaning steps discussed in section 2.2.2, de-ionized millipore water was used. For all the steps involving contact with the samples (last step cleaning, acid dilutions,...) ultrapure milli-Q® Element water with a  $18.2\text{ M}\Omega\cdot\text{cm}^{-1}$  resistivity was used.
- Chemicals: For regular use, reagent grade acids (nitric acid,  $\text{HNO}_3$ ; hydrochloric acid,  $\text{HCl}$ ; hydrofluoric acid,  $\text{HF}$ ) and solvents (acetone,  $\text{C}_3\text{H}_6\text{O}$ ; ethanol,  $\text{C}_2\text{H}_6$ ) were ordered from Merck™.
- High purity acids: For all steps involving sample contact, distilled acids were used. The acids were distilled in a subboiling PicoTrace® cupola distillation system. Acids blanks were checked regularly and the blank contribution of the in-house distilled hydrochloric acid was estimated to be too high, therefore certified Seastar™ Baseline®  $\text{HCl}$  was used instead.

### 2.2.2 Cleaning procedures:

To avoid all contamination from previous samples or from any other source a special cleaning procedure was adopted for all the PFA (PerFluoroAlkoxy) and PTFE (PolyTetraFluoroEthylene) labware:

1. Pre-cleaned with ethanol to remove potential residues.
2. Boiled in a freshly made *aqua-regia* bath (1 vol.  $\text{HNO}_3$  : 3 vol.  $\text{HCl}$ , reagent grade) for 12 hours. This highly oxidizing solution dissolves most of the trace elements and metals effectively.
3. Boiled in a 50% (vol.)  $\text{HCl}$  bath for another 12 hours. This step ensures that all possible active *aqua-regia* is removed.
4. Beakers filled with a mixture of concentrated nitric acid and hydrofluoric acid and kept on a hot plate for two to four days. Other PFA-ware was also cleaned in the same way in big containers.
5. Finally, the beakers were thoroughly rinsed with milli-Q® Element water and dried under laminar flow hoods.

For other non PFA elements, such as pipet tips, another procedure was used:

1. Boiled in de-ionized millipore water bath for 12 hours.

2. Submerged in a warm 10% (vol.)  $HNO_3$  bath for 4 to 8 hours.
3. Submerged in a warm 10% (vol.)  $HCl$  bath for another 4 to 8 hours.
4. Rinsed twice with milli-Q<sup>®</sup> Element water.

### 2.2.3 Clean lab facilities:

All separation steps and sample handling were performed under class 10 laminar flow hoods (High Efficiency Particulate Air filters, HEPA) within a clean lab environment (class 10 000).

## 2.3 Elemental separation scheme

### 2.3.1 Principles of ion exchange chromatography

Before analysis by one of the methods described earlier (c.f. 2.1 - p.16) the samples have to be purified and the different elements preconcentrated and separated. Complete separation decreases the possible negative effects on measurement due to isobaric interferences (different elements with the same atomic number, c.f. 2.4.1 - p.26). These separation steps also ensure that the species are separated from other matrix elements (such as calcium, iron, magnesium, ... ) that can change ionization efficiency and beam focusing in the MS.

These separation and preconcentration steps are commonly achieved by the use of ion exchange resins. Resins allow the reversible exchange of ions between the resin and a liquid phase containing the ions. The resin is packed onto a vertical column and the dissolved sample introduced at the top. The sample solution is allowed to flow by gravity through the column and during that time, ions can be exchanged between the resin and the solution. The different ions have different affinities with the resin and by changing the acid concentration, the type of acid or the amount of acid that passes through the column it is possible to retain and separate the ions and collect the purified species.

Resins are made of an inert solid substrate to which functional groups have been attached. Depending on the functional group used, resins are selective to anions or cations, for instance standard strong acid cation exchange resins are made of a cross-polymerized styrene and divinylbenzene matrix with sulphonic acid ( $-SO_3^- \cdot H^+$ ) as functional groups.

The ion selectivity of a resin depends on different factors, like the degree of electrostatic interaction between the resin's functional group and the solvated ion.

This is a function of the ion charge (multiple charged ions will, in general, be more selected onto the resin due to electrostatic forces) and the size of the solvated ion (that increase with decreasing size of the ion, as the electrostatic field created by a small ion is larger and induces a larger solvation sphere), with smaller solvation spheres being selected more easily by the functional groups. Other parameters also influence the selectivity of the resin such as the swelling of the resin, the interaction with counter-ions and the pore size of the resin but these are beyond the scope of this work and more information can be found in Potts (1987) or Korkisch (1988). The ion selectivity is often expressed as  $k'$  that is proportional to the distribution ratio of the considered specie between the resin and the eluting acid (with a high  $k'$  meaning a high affinity for the resin).

### 2.3.2 A four step separation scheme

The method developed here aims at the separation and preconcentration of the the isotopes analyzed for this study, *i.e.* Sr, Nd, Pb and Hf, but also for another study (c.f. appendix C - p. XIV) using uranium series isotopes and necessitating the analysis of uranium (U), thorium (Th), protactinium (Pa) and radium (Ra), through 4 ion exchange columns (c.f. 9 - p.24).

#### Rock standard digestion and preparation:

Before separation on the columns, the samples were digested in capped small pre-cleaned PFA beakers (c.f. 2.2.2 - p.21) with  $\sim 1$ ml of concentrated ultra-pure  $HNO_3$ ,  $\sim 0.5$ ml of concentrated ultra-pure  $HF$  and a few drops of perchloric acid ( $HClO_4$ ) and warmed on a hot plate for 48 hours. The  $HNO_3$  is a powerful oxidizer and ensures that all salts are kept in solution whereas the  $HF$  volatilizes the silicate fraction as silicon tetrafluoride ( $SiF_4$ ). Perchloric acid was used to oxidize all organic compounds and was found to be more efficient than hydrogen peroxide ( $H_2O_2$ ), although it should be handled with extreme care. After full digestion the samples were dried down and brought into solution in 10N  $HCl$ . Boric acid ( $B(OH)_3$ ) was added to each sample to prevent the formation of insoluble fluorides that might precipitate some elements to be analyzed.

*Remark: For the first separations attempts, ascorbic acid ( $C_6H_8O_6$ ) was added to each sample to reduce the iron and prevent it's competition on the column with other substances such as uranium. But the acid's blank contribution was judged to high and the ratio of the amount of resin to sample size was large enough to compensate for these effects.*

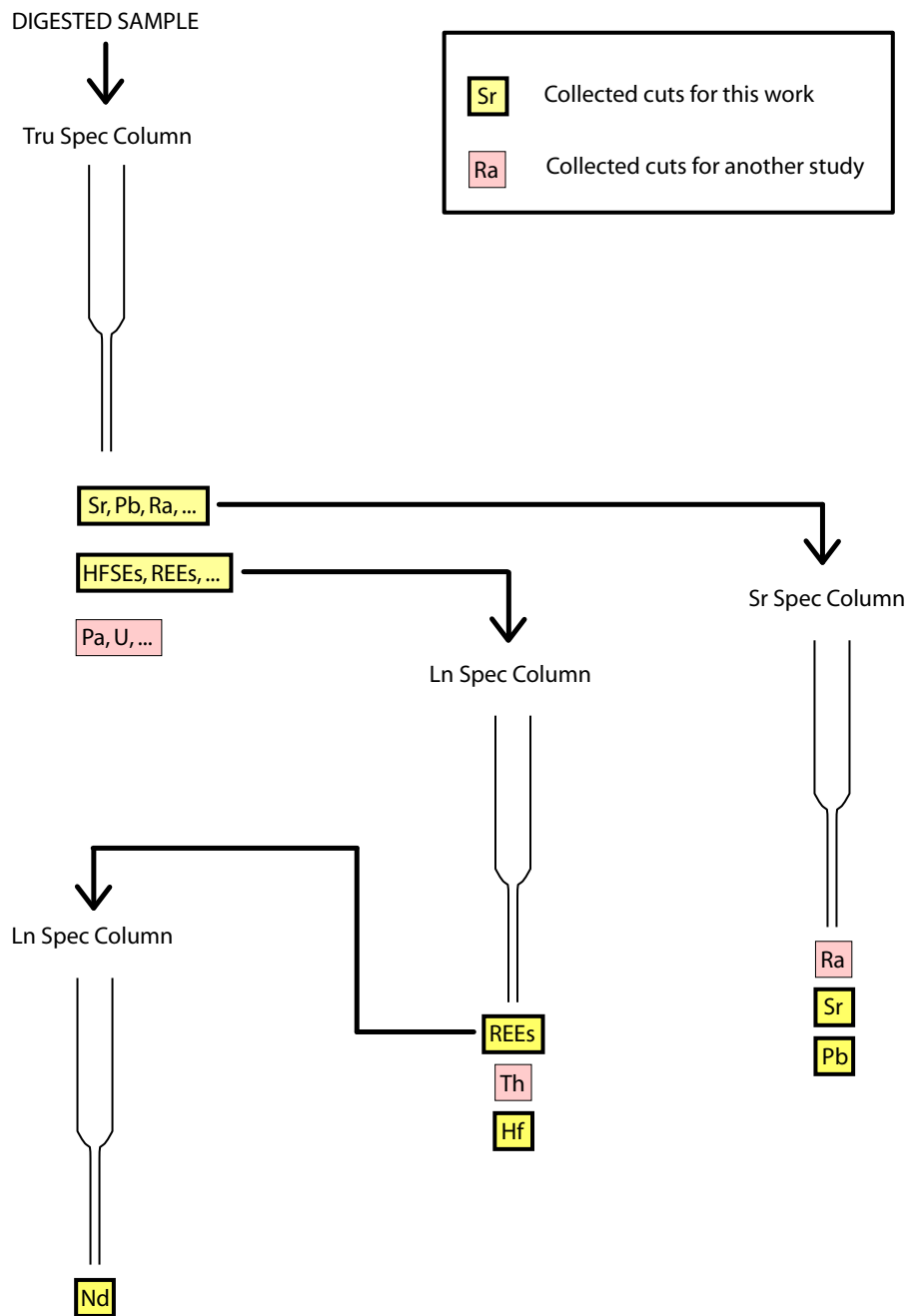


Figure 9: Elemental separation scheme.  
 HFSEs: High Field Strength Elements; REEs Rare Earth Elements.

**Adopted procedures for separation:****TRU-spec column:**

After complete digestion the sample was processed through a TRU-spec ion-exchange column to split the sample in three cuts. The first cut, containing the Sr, Pb and Ra fractions, was eluted in 10N *HCl*, the second cut, containing the High Field Strength Elements (HFSEs) and the Rare Earth Elements (REEs), was eluted in 1N *HCl* and the last cut, containing the U and Pa fractions, was eluted in 0.1N *HCl* - 1N *HF*. The method used was adapted from Goldstein & Stirling (2003) and detailed information on the elution acids and techniques used can be found in the appendix B (p.VI).

The Eichrom<sup>TM</sup> TRU-spec resin (50-100 $\mu$ m mesh) was loaded in cleaned PFA columns with a 500 $\mu$ l reservoir and changed after every use. The columns were calibrated using certified standard solutions of known concentration containing both the trace elements under investigation and the major elements that can negatively effect elution chemistry and sample measurement. The final elution curves were tested with dissolved rock standards of varying composition and concentrations to account for possible changes in matrix effects. The elution curves have been determined using ICPQMS (c.f. 2.1.1 - p. 16).

**Sr<sup>TM</sup>-spec column Ra/Sr/Pb separation:**

The first cut collected from the TRU-spec elution was dried down and brought into solution in 3N *HNO*<sub>3</sub> before loading on a Sr-Spec column. The Eichrom<sup>TM</sup> Sr-spec resin (50-100 $\mu$ m mesh) was loaded in pre-cleaned PFA columns with a 100 $\mu$ l reservoir changed after every use.

Ra was eluted in 3N *HNO*<sub>3</sub>, Sr eluted in 0.05N *HNO*<sub>3</sub> after rinsing Ba in 7.5N *HNO*<sub>3</sub> and Pb was eluted in 6N *HCl*. This method was based on the work of Pin & Zalduegui (1994) and Vajda *et al.* (1997) and for complete information regarding the elution scheme refer to appendix B (p.VI). For more information about Sr spec resin and the selectivity coefficients consult Horwitz *et al.* (1992). Sr yields were over 98%.

**Ln-spec column REEs/Th/Hf separation:**

The second eluted cut from the TRU-Spec was loaded directly on an Eichrom Ln-spec column. The Eichrom<sup>TM</sup> Ln-spec resin (50-100 $\mu$ m mesh) was loaded in pre-cleaned PFA columns with a 700 $\mu$ l reservoir and changed after every use.

Based on the work of Munker *et al.* (2001), we developed a new method to separate the REEs, Th and Hf. After eluting the REEs in 1.2N *HCl*, ytterbium (Yb), lanthanum (La) and titanium (Ti) were rinsed off the column and thorium (Th) eluted in 3N *HCl* - 0.1N *HF* acid. Finally, after rinsing the zirconium (Zr), hafnium (Hf) was eluted in 6N *HCl* - 0.3N *HF*. Complete information can be

found in appendix B - p.VI.  
Hf yields were over 96%.

*Remark: Special care should be observed in the elution of Yb as it has a direct interferences with  $^{166}\text{Hf}$ , which increases the error in the measurement of Hf isotopes. In order to minimize the correction on Hf, the columns were rinsed with large amounts of 6N and 3N HCl.*

### **Ln-spec column Sm/Nd separation:**

The REEs, collected from the previous Ln-Spec column, was loaded in 0.05N  $\text{HNO}_3$ , after drying down, onto a 2nd Ln-spec column were the REEs are separated. After rinsing lanthanum (La), cerium (Ce) and protactinium (Pr), Nd was eluted in 0.3N HCl. Subsequently the Sm was eluted in 1N HCl. The Nd and Sm fractions had to be well separated because Sm has isobaric interferences on many of the Nd isotopes (c.f. 2.4.1 - p.26). The resin was loaded onto a tall 2000 $\mu\text{l}$  column and compacted to ensure a better separation. The columns were calibrated individually and thoroughly cleaned before re-use. Nd yields were over 72% but this value is though to be affected by a manipulation error and could be improved.

*Remark: The elution curves of these columns are sensitive to acid normality, therefore the acid need to be titrated and adjusted carefully. For some applications, collection of the Sm fraction might be necessary, indeed for older rocks, the radiogenic decay of Sm into Nd becomes significant (c.f. 5 - p.32) and an age correction must be applied to determine the original isotopic composition. Therefore, we determined the elution volumes for quantitative Sm collection.*

## **2.4 Isotopic systems**

### **2.4.1 Definitions and methods**

The isotopes measured for this work will be introduced in this section, along with the methods used during their measurement. First, some concepts are introduced.

#### **Isobaric interferences**

Among the elements analyzed, some species with different number of protons have equal mass, *i.e.* the same amount of nucleons (protons + neutrons), such as  $^{87}\text{Sr}$  and  $^{87}\text{Rb}$ . Even if their chemical properties are different, the mass difference is small (as the weight of protons and neutrons are only slightly different). If the mass difference is too small for the mass spectrometer to resolve, the instrument

will detect both species as the same mass; when mass 87 is monitored, the measured intensity is the sum of  $^{87}\text{Sr}$  and  $^{87}\text{Rb}$ .

For elements having more than one isotope, it is possible to correct for this interference by measuring other non-interfering isotopes. Many interfering species have isotopes on masses where no other species does (in the case of Rb,  $^{85}\text{Rb}$  is not interfering with other isotopes). By measuring the abundance of the latter isotope, and assuming the isotopic ratios are well known, it is possible to subtract the appropriate correction factor.

*Formally: if  $^nX$  has to be measured accurately, and  $^nX$  is interfering with  $^nY$ , it is possible to derive the contribution of  $^nY$  to the total " $n$ " beam, by monitoring another isotope of  $Y$ ,  $^pY$ , that has no interferences if the ration  $^nY/^pY$  is known:*

$$^nX_{\text{Corr}} = ^nX_{\text{Meas}} - (^pY \cdot \frac{^nY}{^pY}) \quad (1)$$

### Mass fractionation

During the measurement, physical or chemical processes can affect the isotopes of an element differently, resulting in inaccurate isotopic ratios if not taken into account. For instance during TIMS measurements, the measured ratio varies systematically with time because the rate of evaporation of lighter isotopes is higher than for the heavier species. Hence, the lighter isotope gets depleted in the un-evaporated fraction of the sample and so the heavy isotope / light isotope ratio increases with time. In ICP mass spectrometers, mass fractionation is independent of the amount of initial starting material because the sample is continuously injected into the instrument. However, mass fractionation does occur, primarily during the transfer through the cones and lens stack. Therefore, corrections for mass fractionation must be made in both TIMS and ICPMS measurements.

- **Internal mass fractionation correction**, is applied when the measured element has more than one stable isotope, *i.e.* that is not radiogenic. The ratio formed by these stable isotopes is assumed to be constant regardless of the sample's origin. For heavy elements, the relative mass difference between the isotopes is small enough to neglect fractionation during chemical processes; the isotopic ratio thus remains the same and is inherited from early nucleosynthesis. By measuring the stable ratio simultaneously with the ratio of interest, and comparing the measured value to the true value it is possible to determine the mass fractionation factor of the measured isotopes.

Many fractionation laws have been derived, and the most widely used is an empiric exponential law, based on the assumption that fractionation is governed by a suitable fractionation coefficient  $\beta$ , which relates the masses of the two species of the fractionated ratio to the observed ratio.  $\beta$  is calculated based on the measured and true stable ratio (equation 2) and is then applied to the unknown ratio (equation 3):

$$\beta = \frac{\ln(R_{Meas}^{i,j} - R_{True}^{i,j})}{\ln(m_i - m_j)} \quad (2)$$

$$\implies R_{Corr}^{k,l} = R_{Meas}^{k,l} \cdot \left(\frac{m_k}{m_l}\right)^{-\beta} \quad (3)$$

where

$R_{Meas}^{i,j}$ ,  $R_{Meas}^{k,l}$  the measured ratio of isotope i and j, resp. k, l  
 $R_{True}^{k,l}$  the true ratio of i and j  
 $R_{Corr}^{k,l}$  the corrected ratio of k and l  
 $m_x$ , the mass of isotope x

- **External mass fractionation correction**, is applied when no or only one isotope is stable (e.g., Pb, c.f. 18 - p.II). In this case, the normalization is done by regularly measuring samples with a known isotopic concentration (standards) in conditions as close as possible to the unknown samples. The mass fractionation law is then determined on the standard runs and applied to the unknowns. This method is not as precise as an internal mass fractionation correction because it is difficult to reproduce the same experimental conditions between a standard and a sample and yields less precise results. One solution to overcome this problem is to add a known amount of other isotopes (a double or triple spike) with known isotopic composition and concentration to the sample and measure the resulting isotopic ratios. The added spike is then used to determine an internal mass fractionation correction.

### Isotope dilutions

Isotope dilution is a method employed to measure the concentration of an element (or isotope of an element) if there is a small amount of sample and/or high precision is required. In this technique, a known amount of spike is added to the sample and the ratio of the spike isotopes to sample isotopes measured. The concentration of the sample can then be calculated:

$$\left(\frac{X}{Y}\right)_{Meas} = \frac{X_{Spike} + X_{Sample}}{Y_{Spike} + Y_{Sample}} \quad (4)$$

### 2.4.2 Strontium - Sr

**Isotopes** Strontium - Sr is an alkaline earth metal with atomic number 38. Sr is the 15th most abundant element on earth and is found in many minerals. Because the atomic radius is close to the radius of calcium, Sr substitutes easily for Ca in minerals. Sr has four natural stable isotopes of which only  $^{87}\text{Sr}$  is radiogenic and produced by  $\beta$ - decay (electron emission of the nucleus) of  $^{87}\text{Rb}$  (with a half life of  $4.88 \times 10^{10}$  years).

Isotope	$^{84}\text{Sr}$	$^{86}\text{Sr}$	$^{87}\text{Sr}$	$^{88}\text{Sr}$
Abundance	0.0056	0.0986	0.07	0.8258

Table 1: Strontium isotopes natural abundances.

Therefore, the abundance of  $^{87}\text{Sr}$  in a closed system is a function of the initial amount of  $^{87}\text{Sr}$ , the Rb/Sr ratio and the half life of  $^{87}\text{Rb}$ . The abundance of  $^{87}\text{Sr}$  is commonly normalized to the nonradiogenic  $^{86}\text{Sr}$  and the ratio  $^{87}\text{Sr}/^{86}\text{Sr}$  is a characteristic of a given geographical area. Sr has extensively been used in geochronology since the early sixties, but it has also proven to be a useful tracer for surface processes (e.g., Capo *et al.* (1998) and references therein).

**Mass spectrometry** Sr isotopes are commonly investigating using TIMS (c.f. 2.1.3 - p.19) especially for small samples. For ICP-MS work, the isobaric interferences from doubly charged Ar in the plasma source decreases precision and accuracy; results obtained by TIMS machines has been shown to be higher (Waight *et al.*, 2002).

**Loading** Sr samples were dried down and brought into solution in approximately  $1\mu\text{l}$  of concentrated  $\text{HNO}_3$ . The sample was loaded onto a single filament together with  $1\mu\text{l}$  tantalum (Ta) activator, following the method described by Birck (1986). The sample and activator were loaded, alternating sample and activator layers, onto a zone refined rhenium (Re) filament at a current of approximately 500mA. Filaments were acid cleaned and outgassed for two hours at 4A before use. Once the sample was fully loaded, the filament was heated up slowly to until dull glowing red (approx. 2.2A) for approximately 10 sec. The filament temperature was then lowered and a drop of activator added to limit the

possible loss of sample off the filament during handling.

### Cup configuration

Farraday cup	L1	C	H1	H2	H3
Sr isotope	$^{84}\text{Sr}$		$^{86}\text{Sr}$	$^{87}\text{Sr}$	$^{88}\text{Sr}$
Interferences		$^{85}\text{Rb}$		$^{87}\text{Rb}$	

Table 2: Cup configuration for Sr analysis.

**Measurement procedure** The measurement, performed in static mode using the  $^{88}\text{Sr}$  as control beam for focusing, peak centering and reported beam intensities. Before heating the filament, a baseline measurement (SEM deflection on) was performed for 250 seconds. For certified standard solutions and rock standards, the filament was heated up at  $250^\circ\text{C}/\text{min}$  (analyzer gate closed) until approximately  $1250\text{-}1300^\circ\text{C}$ , allowing residual Rb to burn off (the evaporation temperature of Rb being lower than for Sr). The filament was then heated up until a beam of  $\sim 10\text{mV}$  was detected then a first automatic focusing performed before heating up to  $50\text{-}100\text{mV}$ , the focusing repeated and a peak center performed. The sample was measured when a suitable beam intensity reached (depending on the load) and for samples larger than  $5\text{ng}$ , the filament's temperature was automatically controlled to maintain beam size in a window of 80% to 120% of the initial beam.

Measurements	Integration time	Blocks	Cycles	Inter-block actions
400	4sec	20	20	Focusing every 5 blocks ( <i>samples &gt; 5ng</i> )

Table 3: Measurement procedure for Sr

If the beam intensity dropped below a minimum threshold that decreased the precision, the measurement was stopped and the data re-processed manually.

The ice and dust samples were measured using the same scheme with manual operator control of the measurement, and adjustments made depending on the variation in beam intensity. The measurement was started at lower beam sizes ( $\sim 50\text{mV}$ ) and the temperature increased slowly to attain an optimal precision.

**Mass fractionation and interference corrections** The cup configuration shown in table 2, allowed an accurate measurement of the  $^{87}\text{Sr}/^{86}\text{Sr}$ . An internal mass fractionation correction was applied using the exponential law with the  $^{87}\text{Sr}/^{86}\text{Sr}$  ratio normalized to  $^{88}\text{Sr}/^{86}\text{Sr}$  (8.375209). Rubidium interferences were corrected for by measuring  $^{85}\text{Rb}$  and assuming  $^{87}\text{Sr}/^{85}\text{Rb} = 0.386$ .

**Standard results - NBS987** During the whole duration of this work the NBS987 Sr standard ( $^{87}\text{Sr}/^{86}\text{Sr} = 0.710245$ ) was run regularly using different loading amounts in order to assess the long term reproducibility of the machine and the procedure used.

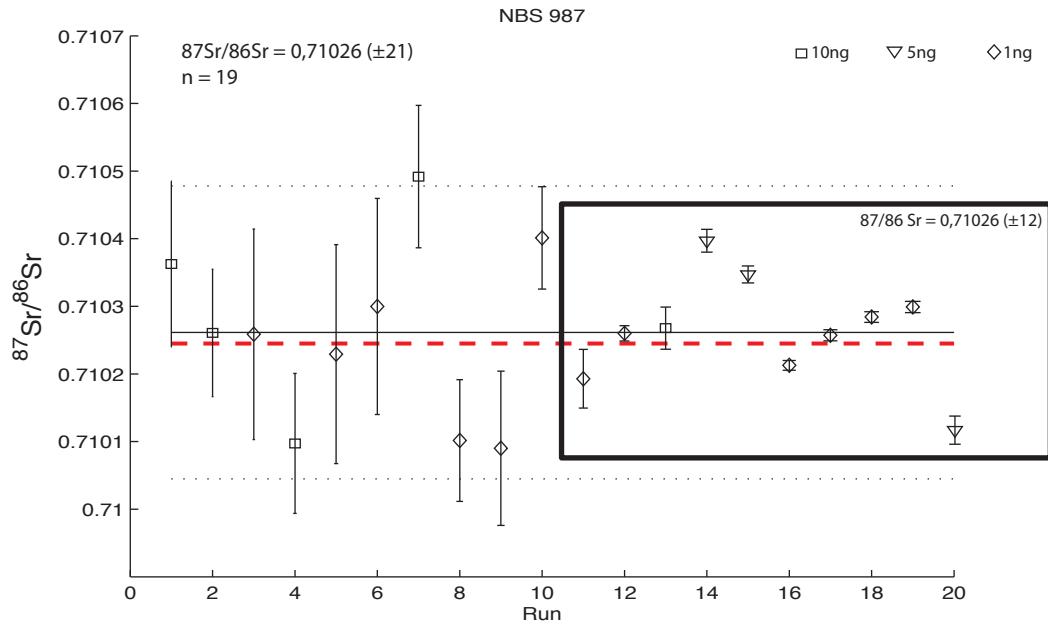


Figure 10: Sr NBS987 runs

Standard results for 10 to 1ng sample sizes. Solid line: mean measured value, dotted line: 2 standard deviation envelope, dashed red line: certified NBS987 value. Ice samples were run during the period outlined from run 11 to 19 where higher precision was achieved.

*Remark:* These results show a net decrease in time of the standard error of single measurements, explained by (1) the improvement in the loading technique skills of the operator and (2) the decision to run the samples for shorter time but with larger beam sizes which significantly increased the precision. The internal and

	$^{87}\text{Sr}/^{86}\text{Sr}$	2Stddev	n	Ext. (ppm)	Mean int. (ppm)
<b>All runs</b>	<b>0.71026</b>	<b>0.00021</b>	<b>20</b>	<b>305</b>	<b>95</b>
10ng	0.71029	0.00029	5	408	128
5ng	0.71024	0.00017	12	241	100
1ng	0.71028	0.00029	3	420	24
run 11-20	0.71028	0.00012	10	162	20

Table 4: Sr NBS987 results

2StdErr defined as  $2\text{stddev}/\sqrt{n}$ ; Ext: external reproducibility as  $2\text{Stddev}/\text{Average}$ ; Mean int.: Mean internal reproducibility of every measurement as  $2\text{StdErr}/\text{Average}$ .

*external reproducibility of the 10ng samples was overall higher, as most of these samples were measured during the first time of this work, when Sr beam intensities were kept low. The ice samples were measured during the period of run 11 to 19 where the external reproducibility had dropped to 162 ppm.*

### 2.4.3 Neodymium - Nd

**Isotopes** Neodymium - Nd is a rare earth metal, with atomic number 60 and constitutes around 38 ppm of the earth's crust.

Nd has 5 natural stable isotopes and 2 radioisotopes,  $^{144}\text{Nd}$  decaying to  $^{140}\text{Ce}$  through the emission of an  $\alpha$  particle (half-life:  $2.29 \times 10^{15}$  year) and  $^{150}\text{Nd}$  decaying to  $^{150}\text{Sm}$  by double  $\beta$ - decay.

Isotope	$^{142}\text{Nd}$	$^{143}\text{Nd}$	$^{144}\text{Nd}$	$^{145}\text{Nd}$	$^{146}\text{Nd}$	$^{148}\text{Nd}$	$^{150}\text{Nd}$
Abundance	0.272	0.122	0.238	0.083	0.172	0.057	0.056

Table 5: Neodymium isotopes natural abundances.

Similar to  $^{87}\text{Sr}/^{86}\text{Sr}$ , the  $^{143}\text{Nd}/^{144}\text{Nd}$  ratio can be used as an indicator of source material or location. Because the variation in the  $^{143}\text{Nd}/^{144}\text{Nd}$  ratio are small, Nd ratios are often reported in  $\varepsilon$  units, which is the deviation of the 143/144 ratio relative to a standard ratio, the CHondrite Uniform Reservoir (CHUR) with  $^{143}\text{Nd}/^{144}\text{Nd} = 0.512638$  (DePaolo & Wasserburg, 1976):

$$\varepsilon_{\text{Nd}} = \left( \frac{(^{143}\text{Nd}/^{144}\text{Nd})_{\text{Meas}}}{(^{143}\text{Nd}/^{144}\text{Nd})_{\text{CHUR}}} - 1 \right) \cdot 10^4 \quad (5)$$

**Mass spectrometry** Nd measurements were carried out on TIMS (c.f. 2.1.3 - p.19) and run directly as a metal.

**Loading** Nd samples were dried down after collection from the column and brought into solution in  $\sim 1\text{-}2 \mu\text{l}$  of a 1N  $HCl$  - 1N  $HNO_3$  (1:1 vol.) and a trace amount of phosphoric acid ( $H_3PO_4$ ). The sample was then loaded onto a double outgassed (2h at  $\sim 5A$ ) Re filament (the ionization temperature being higher than the evaporation temperature of Nd, the temperature of both the filaments has to be controlled individually). The solution was deposited onto the filament at  $\sim 0.7A$ , the current was ramped up to let the phosphoric acid evaporate, and the filament was then brought to dull red ( $\sim 2.2A$ ) for approx. 10 seconds.

### Cup configuration

Farraday cup	L3	L2	L1	C	H1	H2	H3
Nd isotope	$^{142}\text{Nd}$	$^{143}\text{Nd}$	$^{144}\text{Nd}$	$^{145}\text{Nd}$	$^{146}\text{Nd}$		$^{148}\text{Nd}$
Interferences			$^{144}\text{Sm}$			$^{147}\text{Sm}$	

Table 6: Cup configuration for Nd analysis.

**Measurement procedure** For certified standard solutions and rock standards, the measurement procedure was adapted from Caro *et al.* (2006). The ionization filament was heated first, at  $200^\circ\text{C}/\text{min}$  until a temperature of  $1650^\circ\text{C}$  was read on the pyrometer while an electronic baseline measurement was determined. Then the evaporation filament was heated at  $100^\circ\text{C}/\text{min}$  until a small Nd signal detected and a first focusing performed. The evaporation filament was heated up while the ionization's filament current was controlled to sustain a temperature of  $1650^\circ\text{C}$ . Measurement was started at suitable beam size after peak centering and re-focusing.

Measurements	Integration time	Blocks	Cycles	Inter-block actions
400	4sec	20	20	Focusing every 3 blocks ( <i>samples &gt; 5ng</i> )

Table 7: Measurement procedure for Nd

The ice and dust samples were measured using the same scheme with manual operator control of the measurement, and adjustments made depending on the variation in beam intensity. In most cases, the measurement was started at low beam size  $\sim 30\text{mV}$  to ensure maximum time of data collection and the evaporation

filament heated up to reach an optimum beam size.

**Mass fractionation correction**  $^{143}\text{Nd}/^{144}\text{Nd}$  ratio was normalized to  $^{143}\text{Nd}/^{144}\text{Nd}$  (0.7219) using the power law for internal mass fractionation correction (c.f. eq.2 - p.28).

**Standard results - JNdi-1** To assess long term reproducibility of the instrument and method used, a certified standard solution, JNdi-1, was measured regularly in various loading amounts and the results compared with the literature  $^{143}\text{Nd}/^{144}\text{Nd}$  value 0.512115 ( $\epsilon \text{ Nd} = -10.2$ ) (Tanaka *et al.*, 2000).

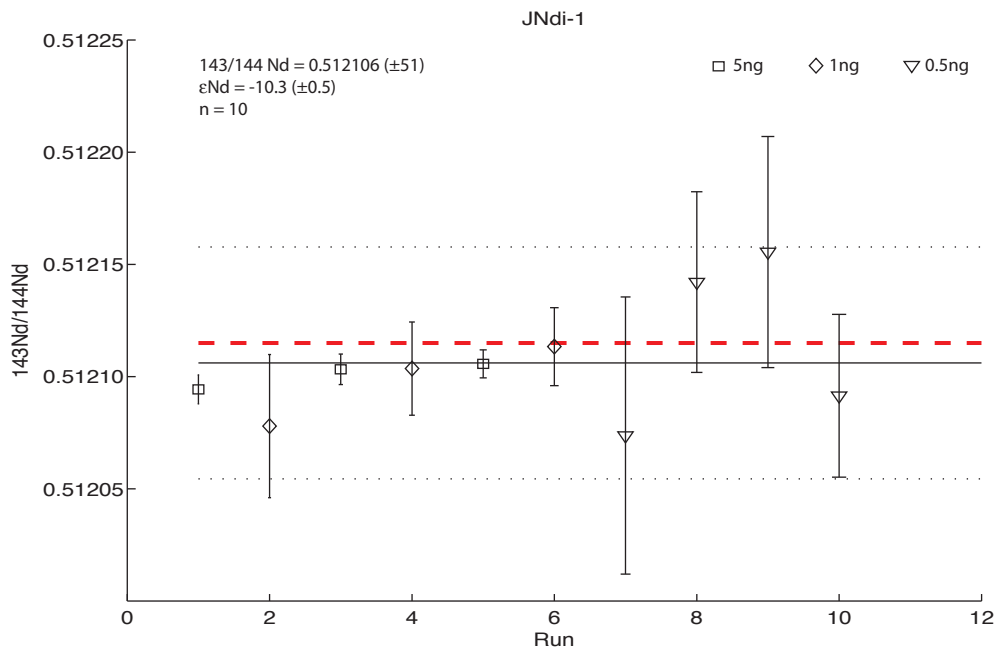


Figure 11: Nd JNdi-1 runs

Standard results for 5 to 0.5ng sample sizes. Solid line: mean measured value, dotted line: 2 standard deviation envelope, dashed red line: certified JNdi-1 value.

#### 2.4.4 Hafnium - Hf

**Isotopes** Hafnium - Hf, element number 72 in the periodic table, constitutes only 0,00058 % of the upper continental crust but is relatively abundant in

	$^{143}\text{Nd}/^{144}\text{Nd}$	<b>2Stddev</b>	$\varepsilon_{Nd}$	<b>n</b>	<b>Ext. (ppm)</b>	<b>Mean int. (ppm)</b>
<b>All runs</b>	<b>0.512106</b>	<b>0.000051</b>	<b>-10.4</b>	<b>10</b>	<b>100</b>	<b>54</b>
5ng	0.512101	0.000012	-9.9	3	24	13
1ng	0.512098	0.000036	-9.9	3	71	45
0.5ng	0.512115	0.000079	-10.2	4	150	92

Table 8: Nd JNdi-1 results

2StdErr defined as  $2\text{stddev}/\sqrt{n}$ ; Ext: external reproducibility as  $2\text{Stddev}/\text{Average}$ ; Mean int.: Mean internal reproducibility of every measurement as  $2\text{StdErr}/\text{Average}$ .

zircons,  $\text{ZrSiO}_4$  (up to 1 - 5%) because of its substitution for zirconium (Zr). Hf has 6 natural isotopes of which  $^{174}\text{Hf}$  is radiogenic and decays to  $^{170}\text{Yb}$  by  $\alpha$ -decay with a half life of  $2 \times 10^{15}$  years.  $^{176}\text{Hf}$  is produced by the  $\beta^-$  decay of  $^{176}\text{Lu}$  with a half-life of  $1.06 \times 10^{11}$ .

Isotope	$^{174}\text{Hf}$	$^{176}\text{Hf}$	$^{177}\text{Hf}$	$^{178}\text{Hf}$	$^{179}\text{Hf}$	$^{180}\text{Hf}$
Abundance	0.00162	0.05206	0.18606	0.27297	0.13629	0.351

Table 9: Hafnium isotopes natural abundances.

Similar to Sr and Nd, the  $^{176}\text{Hf}/^{177}\text{Hf}$  ratio can be used as tracer for provenance and process studies. It was originally applied to mantle geochemistry (Patchett, 1983) and latter to seawater and marine sediments (White *et al.*, 1986).

Hf, like Nd, is often expressed in  $\varepsilon$  units which is the deviation of the 176/177 ratio relative to the CHUR composition: 0.282769 (Patchett, 1983):

$$\varepsilon_{Hf} = \left( \frac{(^{176}\text{Hf}/^{177}\text{Hf})_{\text{Meas}}}{(^{176}\text{Hf}/^{177}\text{Hf})_{\text{CHUR}}} - 1 \right) \cdot 10^4 \quad (6)$$

**Mass spectrometry** Hf was measured on the NuInstrument MC-ICPMS instruments (c.f. 2.1.2 - p.18).

**Loading** After column separation Hf was measured in a 5%*HCl* - 1%*HF* solution.

### Cup configuration

**Measurement procedure** Standard solutions and rock standards were measured in static mode. The NuInstrument was carefully tuned for high sensitivity

Farraday cup	L4	L2	L1	C	H1	H2	H3	H4	H5
Hf isotope		$^{174}\text{Hf}$		$^{176}\text{Hf}$	$^{177}\text{Hf}$	$^{178}\text{Hf}$	$^{179}\text{Hf}$	$^{180}\text{Hf}$	
Interferences	$^{172}\text{Yb}$		$^{175}\text{Lu}$	$^{176}\text{Yb}$ $^{176}\text{Lu}$				$^{180}\text{W}$	$^{182}\text{W}$

Table 10: Cup configuration for Hf analysis.

and stability before and during measurement sessions. A standard bracketing mode measurement scheme was adopted in which every sample is measured in between two certified standard solutions. The measured sample ratio was corrected for the average of the two bracketing standards:

$$R_{Corr}^i = R_{Meas}^i + \left( \frac{\Delta R_{Std}^{i+1} + \Delta R_{Std}^{i-1}}{2} \right) \quad (7)$$

With:

$R_{Corr}^i$ , the corrected sample ratio for a measurement i

$R_{Meas}^i$  the measured sample ratio during measurement i

$\Delta R_{Std}^{i-1}$ ,  $\Delta R_{Std}^{i+1}$  the deviation of the measured standard ratio to the certified value for measurement i-1, resp. i+1.

As a general rule, samples were only measured if  $\Delta R_{Std}^{i-1} < 100\text{ppm}$ . Certified standard and rock standards were measured automatically (measurement routine courtesy J.D. Rickli, IGMR -ETHZ):

Measurements	Integration time	Prior to measurement
25	5sec	30sec baseline peak center

Table 11: Measurement procedure for Hf

Small samples ( $\leq 2\text{ng}$ ) and dust samples were measured using a time resolved software that allowed optimal reprocessing of the data by choosing the measurement interval after the run.

**Mass fractionation correction** The measured  $^{176}\text{Hf}/^{177}\text{Hf}$  ratio was normalized to the constant  $^{179}\text{Hf}/^{177}\text{Hf}$  ratio (0.7325) using the internal, exponential mass fractionation correction law (c.f. eq. 2 - p.28).

**Standard results - JMC475** Long term reproducibility and standard bracketing were assessed by measuring the certified JMC475 solution, with a  $^{176}\text{Hf}/^{177}\text{Hf}$  ratio of 0.28216 ( $\varepsilon_{\text{Hf}} = -21.5$ ).

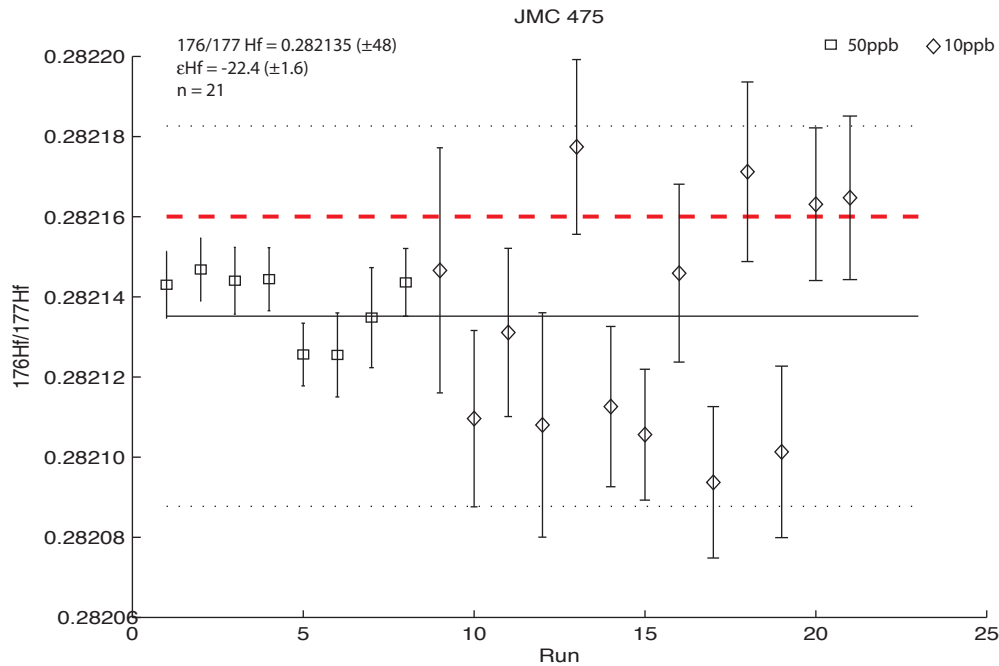


Figure 12: Hf JMC475 runs

Standard results for 50ppb and 10ppb sample solutions. Solid line: mean measured value, dotted line: 2 standard deviation envelope, dashed red line: certified JMC475 value.

## 2.5 Ice processing

### 2.5.1 Decontamination and melting

The ice core sections (approx. 50-60cm) were stored at  $-20^{\circ}\text{C}$  in a dedicated freezer of the IGMR laboratories packed in their original plastic bags. If necessary, ice-core sections were carefully broken in smaller sections within their original bag prior to decontamination.

Decontamination consisted of the removal of the outer layers of snow and ice of the core that were expected to be contaminated while drilling (drilling fluids, oil and other anthropogenic input) and was carried out in systematic steps:

	$^{176}\text{Hf}/^{177}\text{Hf}$	<b>2StdErr</b>	$\varepsilon_{Hf}$	<b>n</b>	<b>Ext. (ppm)</b>	Mean int. (ppm)
<b>All runs</b>	<b>0.282135</b>	<b>0.000028</b>	<b>-22.4</b>	<b>21</b>	<b>84</b>	<b>60</b>
50ppb	0.282138	0.000018	-22.3	8	61	32
10ppb	0.282133	0.000059	-22.5	13	212	78

Table 12: Hf JMC475 results

2StdErr defined as  $2\text{stddev}/\sqrt{n}$ ; Ext: external reproducibility as  $2\text{Stddev}/\text{Average}$ ; Mean int.: Mean internal reproducibility of every measurement as  $2\text{StdErr}/\text{Average}$ .

1. The outer firm layer was removed under clean lab conditions using an acid cleaned, high density PFA chisel fabricated for this purpose. The ice core was left at room temperature for 5 to 10 minutes, and then washed with milli-Q water. A small piece of ice was collected for oxygen isotopic analysis.
2. The core was then moved under HEPA laminar flow hoods, where all further steps were carried out. The core was placed on a clean PFA holder and scraped with a second, clean, PFA chisel to remove the outer ice layers before rinsing thoroughly with milli-Q water.
3. A second scraping and rinsing was performed before placing the core in a pre-cleaned 2L PFA beaker.
4. The ice was then melted under an infrared lamp and the melt water buffered to a neutral pH with ultra-clean EthyleneDiamineTetraAcetic acid (EDTA) and Seastar<sup>TM</sup> Baseline Ammonia ( $NH_3$ ). EDTA is complexing prevents the adsorption of ions already in solution onto the dust particles while ammonia prevents leaching ions out of the dust due to the acidity of the pure ice water (pH approximately 5).

### 2.5.2 Filtering

After melting the liquid was immediately processed and filtered. The filtering consisted of a two stage PTFE filter of  $0.2\mu\text{m}$  and  $30\mu\text{m}$ , pressurized under a clean nitrogen gas ( $N_2$ ) flow. Particle fraction smaller than  $0.2\mu\text{m}$  was considered dissolved matter whereas the  $30\mu\text{m}$  filter could collect any potential antropogenic contamination (fibers, etc). Filters were cleaned in individual 60mL PFA beakers, first in aqua regia, then  $HCl$  and then concentrated  $HNO_3$ ,  $HF$  and perchloric acid. Finally, the filters were rinsed and stored in milli-Q water to eliminate all traces of cleaning acids.

Immediately before use, the filters were wetted with distilled ethanol and subsequently 1 liter of milli-Q water was processed through the filter before filtering

samples in order to wash away any traces of ethanol.

### 2.5.3 Sample dissolution

**Dust fraction:** the 30  $\mu\text{m}$  filter was discarded and the 0.2 $\mu\text{m}$  was put on a hot-plate in a PFA beaker with  $\sim 1\text{ml}$  conc.  $\text{HNO}_3$ , 0.5ml conc.  $\text{HF}$  and 2-3 drops of perchloric acid, then the solution decanted after 2 days. Then approximately 1ml of 6N  $\text{HCl}$  was added to the filter, the beaker capped, digested, and decanted after a day and the operation repeated. The total decanted liquid ( $\sim 4\text{mL}$ ) was dried down on a hot plate and processed through the column chemistry 2.3.2 - p. 23.

Dissolution yields were checked with BCR-2 and ATHO rock standards and yielded over 99.9% of the total U. Even though yields were not verified for the other elements studied, U yields are likely to be representative of the other elements within 1%.

**Liquid fraction:** the filtered liquid (2-3 liters) was dried down in HEPA laminar flow hoods under continuous  $\text{N}_2$  flow and infrared light, drying  $\sim 1\text{L} / 24\text{h}$  with minimum contamination. Before complete dryness, 1mL of concentrated  $\text{HNO}_3$  and 0.25 mL of  $\text{HF}$  was added to the beaker which was capped and warmed on a hot plate for 3 to 4 days to digest the EDTA. After drying down, the residue was brought into solution and prepared for ion exchange chemistry.

## 3 Results

### 3.1 Rock standards

Validation and quality control of the method described in section 2 was done using a certified rock standard. Material used was the powdered Columbia River Basalt (BCR-2) issued by the United States Geological Survey (USGS) and collected in 1996 from the Bridal Veil Flow Quarry near Portland, Oregon (US).

The rock standard was measured as an unknown and measurements compared with literature values. The measured rock standard samples were obtained by dissolving the powder in a concentrated  $HNO_3$ ,  $HF$  and perchloric acid solution and were processed through the complete ion exchange chemistry and measured using the methods mentioned in section 2. The samples were prepared from various rock standard dissolution batches.

#### 3.1.1 Strontium - Sr

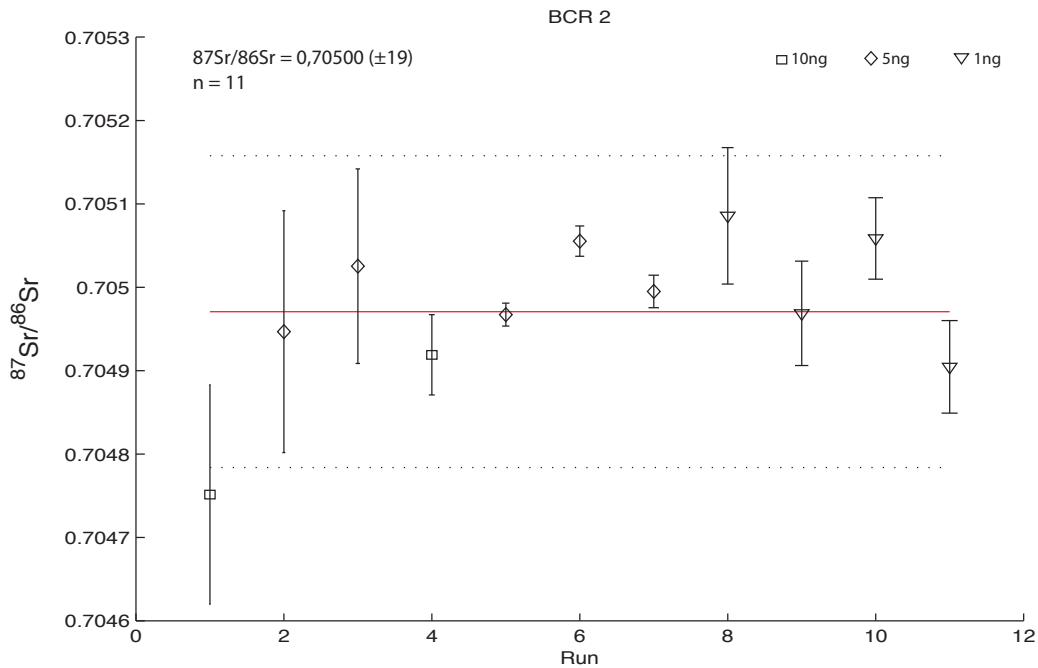


Figure 13: Sr BCR-2 measurements

Standard results for 10, 5 and 1 ng samples of strontium prepared from certified BCR-2 rock standard. Solid line: mean measured value, dotted line: 2 standard deviation envelope.  $^{87}Sr/^{86}Sr$  normalized to NBS987 standard value: 0.710245

$^{87}\text{Sr}/^{86}\text{Sr}$	2Stddev	n	Ext. (ppm)	Mean int. (ppm)
<b>0.70500</b>	<b>0.00019</b>	<b>11</b>	<b>269</b>	<b>96</b>

Table 13: Sr BCR-2 results

2StdErr defined as  $2\text{stddev}/\sqrt{n}$ ; Ext: external reproducibility as  $2\text{Stddev}/\text{Average}$ ; Mean int.: Mean internal reproducibility of every measurement as  $2\text{StdErr}/\text{Average}$ .  $^{87}\text{Sr}/^{86}\text{Sr}$  normalized to NBS987 standard value: 0.710245.

Measured Sr isotopic composition of the BCR-2 standard are in good agreement with literature values: 0.704958(17) (Raczek *et al.*, 2003) and 0.705015(13) (Balcaen *et al.*, 2005). Higher error in the measurements is imputed to the small sample size.

Rb interferences were corrected for and contributed on average to less than 2‰ to the total  $^{87}\text{Sr}$  beam.

### 3.1.2 Neodymium - Nd

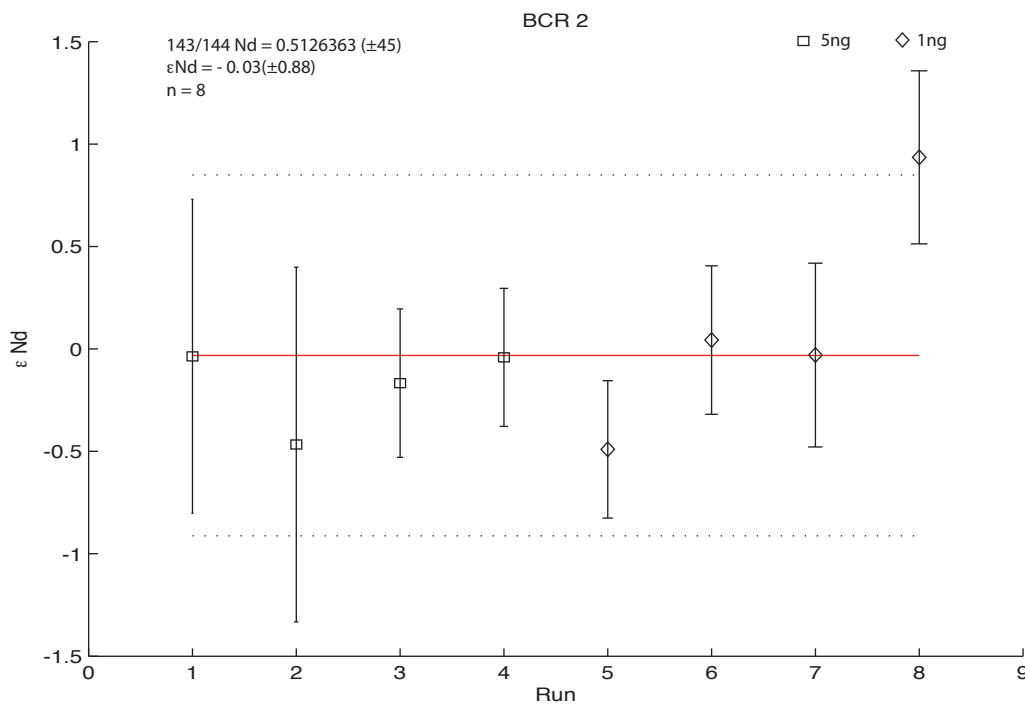


Figure 14: Nd BCR-2 measurements

Standard results for 5 and 1 ng samples of neodymium prepared from certified BCR-2 rock standard. Solid line: mean measured value, dotted line: 2 standard deviation envelope.  $^{143}/^{144}\text{Nd}$  normalized to JNdi-1 standard value: 0.512115.

$^{143}\text{Nd}/^{144}\text{Nd}$	2Stddev	$\epsilon_{Nd}$	n	Ext. (ppm)	Mean int. (ppm)
<b>0.5126363</b>	<b>0.000045</b>	<b>-0.03</b>	<b>8</b>	<b>87</b>	<b>49</b>

Table 14: Nd BCR-2 results

2StdErr defined as  $2\text{stddev}/\sqrt{n}$ ; Ext: external reproducibility as  $2\text{Stddev}/\text{Average}$ ; Mean int.: Mean internal reproducibility of every measurement as  $2\text{StdErr}/\text{Average}$ .  $^{143}/^{144}$  Nd normalized to JNdi-1 standard value: 0.512115.

Neodymium isotopic composition of the BCR-2 standard is measured here is within error of the literature value of Raczek *et al.* (2003): 0.512633(16) ( $\epsilon_{Nd} = -0.098$ ). Higher errors are due to the small sample sizes used. Sm interferences were monitored and corrected for, and contributed to less than 10ppm of the total  $^{144}\text{Nd}$  beam.

### 3.1.3 Hafnium - Hf

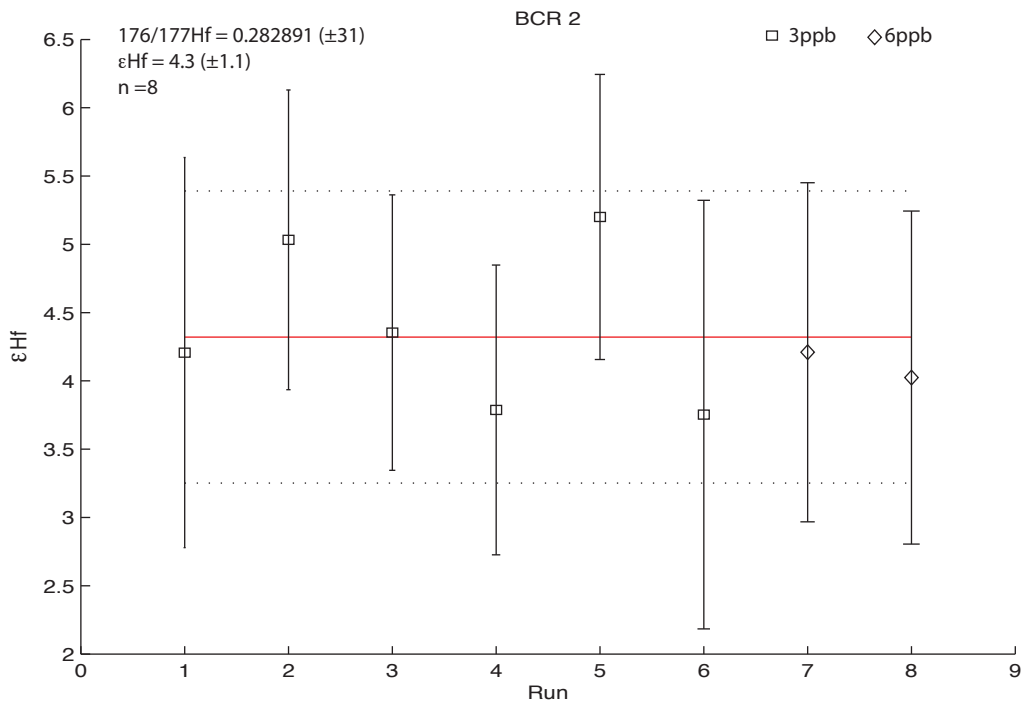


Figure 15: Hf BCR-2 measurements

Standard results for 3 and 6 ppb solutions of hafnium prepared from certified BCR-2 rock standard. Solid line: mean measured value, dotted line: 2 standard deviation envelope.

The measured Hf isotopic composition of the BCR-2 standard is in good agreement with available literature data: 0.282867(18) (Weis *et al.*, 2007);

$^{176}\text{Hf}/^{177}\text{Hf}$	2Stdev	$\varepsilon_{\text{Hf}}$	n	Ext. (ppm)	Mean int. (ppm)
<b>0.282891</b>	<b>0.000031</b>	<b>4.3</b>	<b>8</b>	<b>109</b>	<b>121</b>

Table 15: Hf BCR-2 results

2StdErr defined as  $2\text{stddev}/\sqrt{n}$ ; Ext: external reproducibility as  $2\text{Stdev}/\text{Average}$ ; Mean int.: Mean internal reproducibility of every measurement as  $2\text{StdErr}/\text{Average}$ .

0.282869(14) (Connelly *et al.*, 2006); 0.282895(18) (Hanyu *et al.*, 2005); 0.282888 (LeFevre & Pin, 2001).

Special care was taken to remove Yb and La interferences during ion exchange steps. BCR-2 samples were measured with less than 92ppm Yb and 5ppm Lu contribution to the  $^{176}\text{Hf}$  beam, yielding only minor corrections.

The isotopic results of the BCR-2 standard measurements validate the method used for small size ice and dust samples. The reproducibility and precision achieved allows resolving the isotopic finger prints of different PSAs.

### 3.2 Ice and dust fractions

The Sr, Nd and Hf concentrations and isotopic composition of the Dye-3 dust and ice samples are summarized in Table 17. Six ice core sections have been analyzed for ice and dust isotopic composition and elemental concentrations have been determined on 3 of the sections (130A, 132A and 132B). Hf isotopic composition has been measured on dust samples only, because the concentration in the ice fraction was expected to be too low. Valid Hf isotopic measurements were obtained only for half of the samples (130A, 132A and 132B).

Procedural blanks, including filtration steps and dissolution of the filter were performed regularly during each new sample batch processing (2 to 3 samples) and were measured using isotope dilution methods (c.f. 2.4.1 - p.28).

	Sr (pg)	Nd (pg)	Hf (pg)
Dust	54	3	6
Water	220	20	-

Table 16: Mean procedural blanks

Blank contribution was less than 1% and considered negligible. For the elemental concentrations, a small aliquot ( $\pm 5\%$ ) of the sample was taken, analyzed using isotope dilution methods and corrected for blank contribution.

The dust fraction  $^{87}\text{Sr}/^{86}\text{Sr}$  and  $\epsilon_{Nd}$  composition, plotted in context of PSA characteristics in figure 17, shows distinct compositions of the Dye-3 dust content. Three distinct groups can be identified: (1) samples 129A bot and 130A are characterized by the less radiogenic Sr and most radiogenic Nd isotopic composition of the dust samples. (2) 129B, 130B and 132B exhibit lower  $\epsilon_{Nd}$  values with intermediate Sr compositions. (3) 132A is the most radiogenic Sr sample with intermediate  $\epsilon_{Nd}$  values. Available Hf isotopic composition of dust correlates to the  $\epsilon_{Nd}$  value with sample 130A having a positive  $\epsilon_{Hf}$  value. Concentrations of Sr, Nd and Hf do not show particular patterns: if Sr and Nd are lower for the oldest sample Hf concentrations remain constant. Sr/Nd concentration ratios are between 5.9 and 7 whereas Nd/Hf show more variability (1.5 - 5).

The water fraction isotopic composition is characterized by small variations of  $^{87}\text{Sr}/^{86}\text{Sr}$  (less than 0.0006) but significant variations of  $\epsilon_{Nd}$  (6.8  $\epsilon$  units). Sr composition, unlike Nd, of the water fraction correlates with the isotopic composition of the dust fraction (except for 130A and 130B), more radiogenic water samples being the more radiogenic dust samples and *vice versa*. Concentrations of Sr and Nd are correlated to the dust concentration and vary from simple to

double. The concentration of Sr is 5 to 7 times higher in the water than in the dust fraction whereas Nd and Hf are respectively similar and lower. Sr/Nd and Nd/Hf concentrations are constant, respectively 30 and 10.

Oxygen isotopes were measured by S. Bernasconi (Geological Institute-ETHZ).  $\delta^{18}O$  show large variations of about 5‰ that are typical for winter/summer precipitation alternation. Winter precipitation is characterized by more negative  $\delta^{18}O$ . This data combined to the local accumulation rate allow us to characterize the local stratigraphy and confirms the seasonal to yearly resolution of the measurements.

Table 17: Dust and ice isotopic composition.

Sample	Depth (m)	Size (g)	$\delta^{18}O$ (‰)	Sr (ppt)	Nd (ppt)	Hf (ppt)	$^{87}Sr/^{86}Sr$ $\pm 2\sigma 10^{-6}$	$^{143}Nd/^{144}Nd$ $\pm 2\sigma 10^{-6}$	$\epsilon_{Nd}$ $\pm 2\sigma$	$^{176}Hf/^{177}Hf$ $\pm 2\sigma 10^{-6}$	$\epsilon_{Hf}$ $\pm 2\sigma$
129A	128.3 - 128.6	1298 dust	n.d.	n.d.	n.d.	n.d.	0.712416(337)	0.512290(96)	-6.8(1.9)	n.d.	n.d.
		ice	-30.6	n.d.	n.d.	n.d.	0.709975(15)	0.512163(55)	-9.2(1.1)	n.d.	n.d.
129B	128.6 - 129.0	2594 dust	n.d.	n.d.	n.d.	n.d.	0.717700(42)	0.511932(69)	-13.7(1.4)	n.d.	n.d.
		ice	-27.7	n.d.	n.d.	n.d.	0.710359(10)	0.512339(131)	-5.8(2.6)	n.d.	n.d.
130A	129.0 - 129.6	2886 dust	5.9	1.0	0.2	0.2	0.716440(22)	0.512186(37)	-8.8(0.7)	0.282867(70)	3.4(2.5)
		ice	-26.1	29.0	0.9	0.1	0.710114(18) 0.710123(11)	0.512187(55)	-8.8(1.1)	n.d.	n.d.
130B	129.6 - 130.0	2221 dust	n.d.	n.d.	n.d.	n.d.	0.717021(118)	0.511929(94)	-13.8(1.8)	n.d.	n.d.
		ice	-28.2	n.d.	n.d.	n.d.	0.710008(11)	0.511991(112)	-12.6(2.2)	n.d.	n.d.
132A	131.0-131.5	2854 dust	6.3	0.9	0.3	0.3	0.720226(25)	0.511982(44)	-12.8(0.9)	0.282646(75)	-4.4(2.7)
		ice	-27.6	31.7	1.2	0.1	0.710524(19) 0.710522(22)	0.512051(30)	-11.4(0.6)	n.d.	n.d.
132B	131.5 - 132.0	2986 dust	1.9	0.3	0.2	0.2	0.717407(27)	0.511818(191)	-16.0(3.7)	0.282562(146)	-7.3(5.2)
		ice	-25.4	14.3	0.5	0.1	0.710343(17) 0.710352(19)	0.512140(54)	-9.7(1.1)	n.d.	n.d.

Results are normalized to standard values, Sr NBS987: 0.710245; Nd JNdI-1: 0.512115; Hf JMC: 0.28216. Errors are reported as  $2\sigma$  internal errors.  $2\sigma$  external reproducibility ( $2\text{stdev}/\text{mean}$ ), based on standard results during measurements are: Sr 169 ppm, Nd 100ppm, Hf 84ppm.

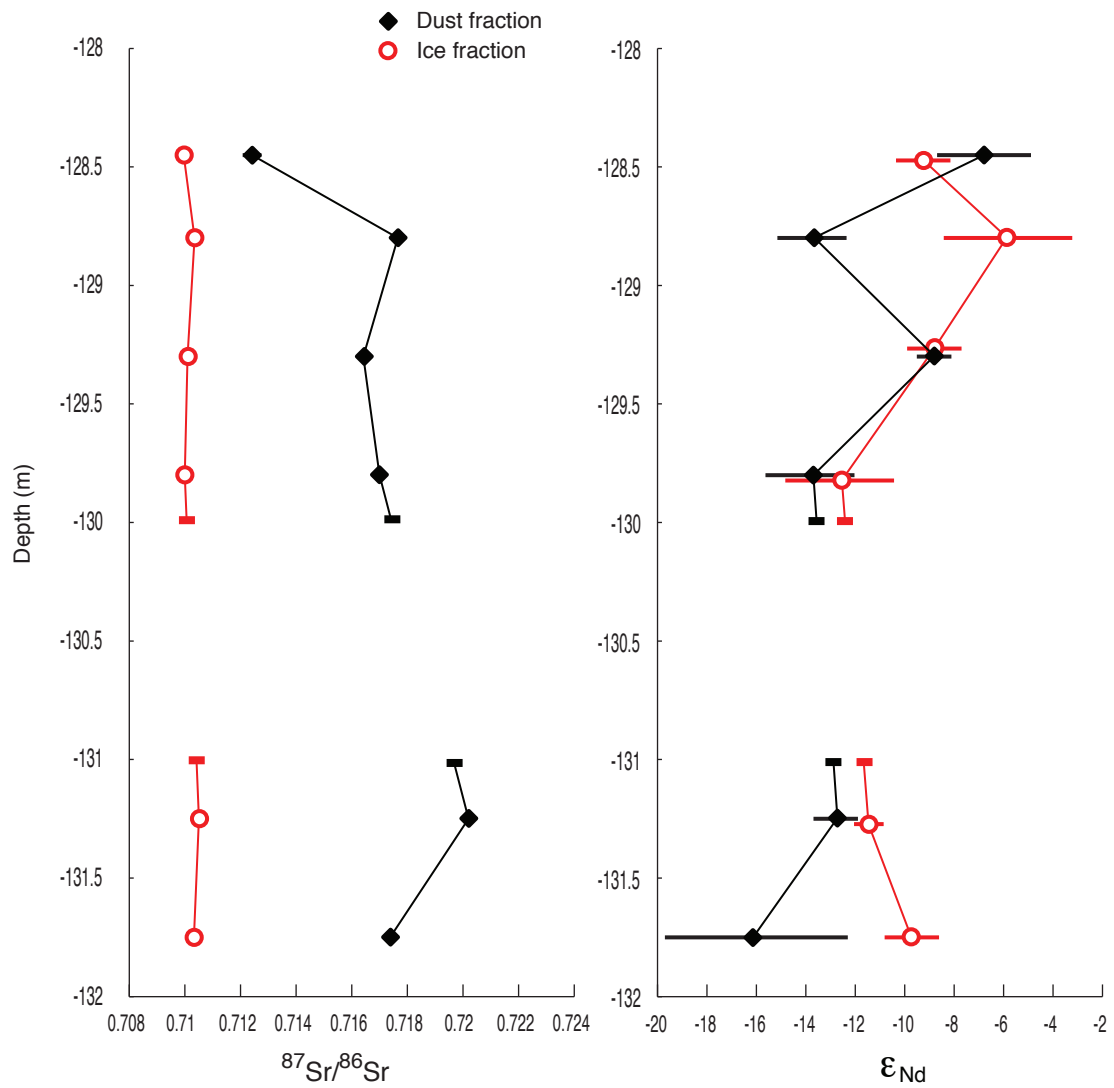


Figure 16: Strontium and neodymium composition of Dye-3 dust and ice fractions as a function of depth.

## 4 Discussion

### 4.1 Dust provenance

The isotopic results of Sr and Nd isotopic composition in the dust extracted from the Dye-3 ice core supports a variability in source area contribution as previously mentioned by Bory *et al.* (2003a). The different composition of the dust samples cannot be explained by variability within one source area as far as the PSA isotopic data available is representative of the whole source area.

Asian sources are likely candidates for the analyzed dust but we observe a general shift towards less radiogenic  $^{87}\text{Sr}/^{86}\text{Sr}$  values. Three possibilities can be proposed for this systematic shift: (1) the contribution of Sr of carbonates in the dust fraction, (2) mixing with some volcanic member with low  $^{87}\text{Sr}/^{86}\text{Sr}$  values or (3) mixing with other source areas.

The PSA samples used for comparison with the Greenland dust fraction have been analyzed after removal of carbonates by acetic acid leaching in order to keep only the silicate fraction. For the samples analyzed in this study leaching was not possible (c.f. appendix C - p. XIV) but the Sr carbonate contribution can be estimated and corrected for using the Sr/Nd concentration ratio of the different dust components.

The mean Sr/Nd ratio found in carbonate free Greenland dust is 3.4 ( $\pm 1$ ) (Svensson *et al.* (2000) and Bory *et al.* (2002)) whereas in this study the Sr/Nd ratio ranges between 5.9 and 7 (mean 6.4) indicating that Sr rich carbonates may have contributed to the overall Sr in the dust fraction (although the leaching procedure used in other studies may also leach Sr adsorbed onto the clay minerals and further change the Sr/Nd ratio). In order to estimate the carbonate fraction, the Sr/Nd ratio of the carbonate in the dust fraction must be known. No data we are aware of directly investigates the Sr and Nd concentrations of carbonates in size fractions under  $5\mu\text{m}$  but typical Sr/Nd in bulk Asian loess carbonates (leachates) range from 20 to 75 (mean  $\sim 40$ ) and is mainly controlled by variations in Sr concentration (Honda *et al.*, 2004). A simple mass balance calculation yields that the contribution of carbonates to the overall Sr budget is smaller than 10 %.

Uranium activity ratios ( $^{234}\text{U}/^{238}\text{U} = \lambda_{234}[^{234}\text{U}]/\lambda_{238}[^{238}\text{U}]$ ) measured on the same dust samples (results not shown here, S. Aciego IGMR- ETHZ) are less than 1, which is typical of a continental weathering environment ( $^{234}\text{U}$  is preferentially leached due to daughter recoil effects). Assuming an average carbonate  $^{87}\text{Sr}/^{86}\text{Sr}$

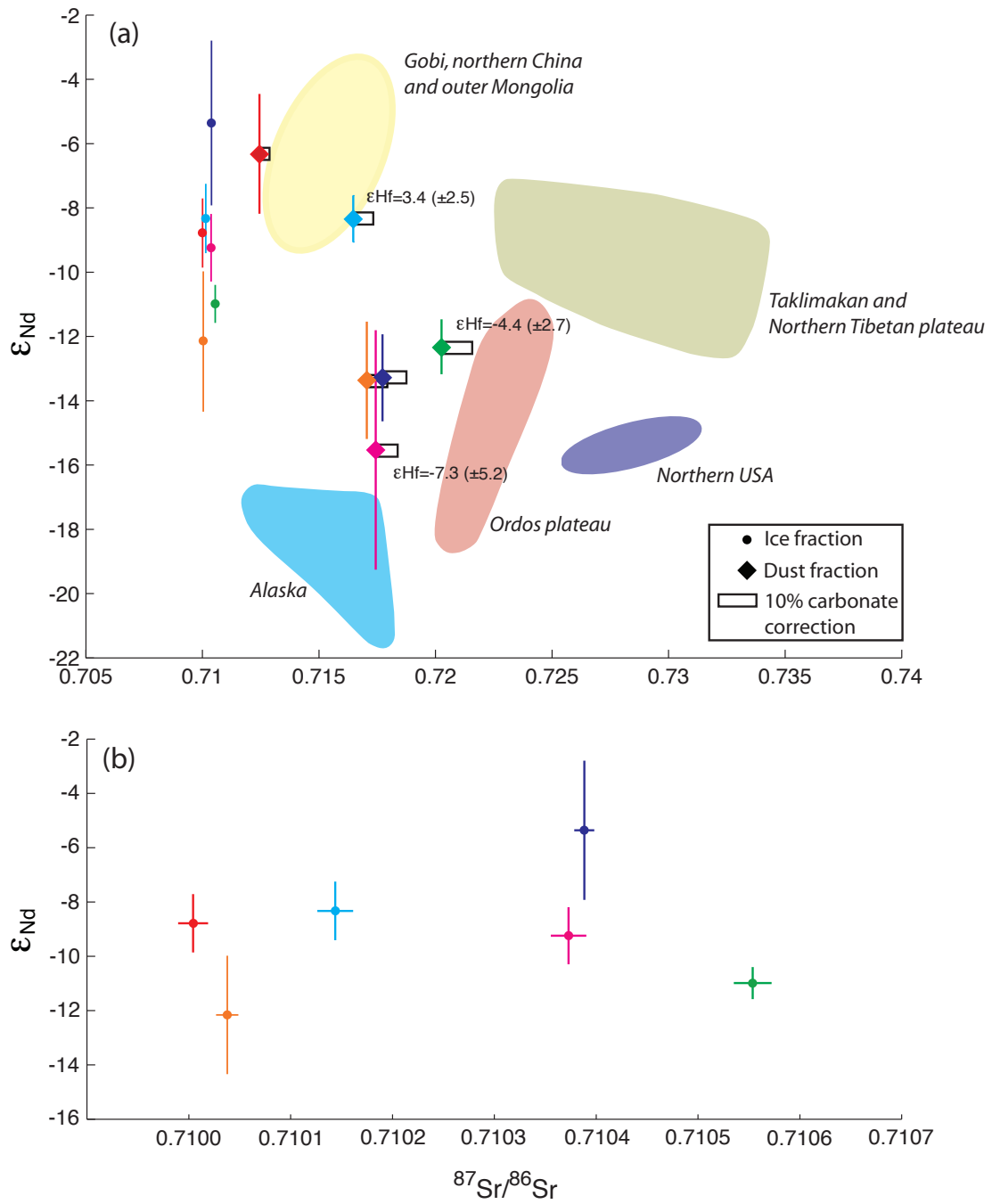


Figure 17: Neodymium and hafnium composition of Dye-3 dust and ice compared to literature data - (a) dust and ice isotopic composition - (b) details of ice isotopic composition.

of 0.7085 (Raymo & W.F., 1992) the measured Sr ratios can be corrected for their carbonate contribution. Using this approach the corrected dust isotopic composition is shifted towards higher  $^{87}\text{Sr}/^{86}\text{Sr}$  ratios by  $\Delta\text{Sr} = 0.00075$  for the least radiogenic sample (130A) to  $\Delta\text{Sr} = 0.0011$  for the most radiogenic sample (132A). No correction has been made to the Nd isotopic ratios, as the contribution of Nd from carbonates to the overall dust is small and leaching experiments have shown close Nd isotopic ratios between bulk and leached PSA samples (Yokoo *et al.*, 2004). Any correction attempt would lie within experimental errors.

As shown in figure 17, the possible carbonate correction is able to explain part of the offset between PSA samples and the dust extracted from the Dye-3 ice core, but it is not sufficient to account for the full difference. This offset is in accord to other literature data, where an offset between PASs and dust samples remains even after carbonate leaching (Biscaye *et al.* (1997); Svensson *et al.* (2000); Bory *et al.* (2003b)).

Mixing of volcanic aerosols is a plausible hypothesis to explain the observed shift toward less radiogenic Sr isotopic ratios. Northern hemisphere volcanic activity is a potential source for mineral aerosols in the atmosphere that may reach as far as Greenland (Clausen *et al.*, 1997). The volcanic aerosols are characterized by non radiogenic  $^{87}\text{Sr}/^{86}\text{Sr}$  and  $\epsilon_{\text{Nd}}$  values and mixing with other dust sources would lead to a shift towards less radiogenic Nd and Sr values. Our Sr, Nd data does not exclude this hypothesis but based on the Hf measurements a significant contribution of 10 to 25% of a volcanic end member, as found in Biscaye *et al.* (1997) is unlikely. The  $\epsilon_{\text{Hf}}$  and  $\epsilon_{\text{Nd}}$  data measured for 132A and 132B is less radiogenic than the asian dust component found in Pettke *et al.* (2002) (c.f. fig 18), and cannot be the result of mixing between asian dust and a volcanic end member. Sample number 130A however plots toward more radiogenic values than average Asian dust, but not directly on a binary mixing model between Asian dust and a volcanic end member which makes it's interpretation in terms of volcanic contribution more difficult. Nevertheless 130A still closely agrees with a purely Asian dust end member (as defined by Pettke *et al.* (2002):  $-10.8 > \epsilon_{\text{Nd}} > -9.0$  and  $-4.7 > \epsilon_{\text{Hf}} > 2.5$ ). The overall shift towards more radiogenic  $\epsilon_{\text{Hf}}$  values compared to the terrestrial  $\epsilon_{\text{Hf}}/\epsilon_{\text{Nd}}$  array of the dust samples thought to be due to sorting during transport or incongruent weathering in the source area.

The influence of other source areas cannot be excluded. According to model studies, Saharan and Arabian contribute up to 75% of the total atmospheric dust load (Tanaka & Chiba (2006) and references therein) but are not represented in the PSA data set available if the data from the greater than  $5\mu\text{m}$  size fractions are

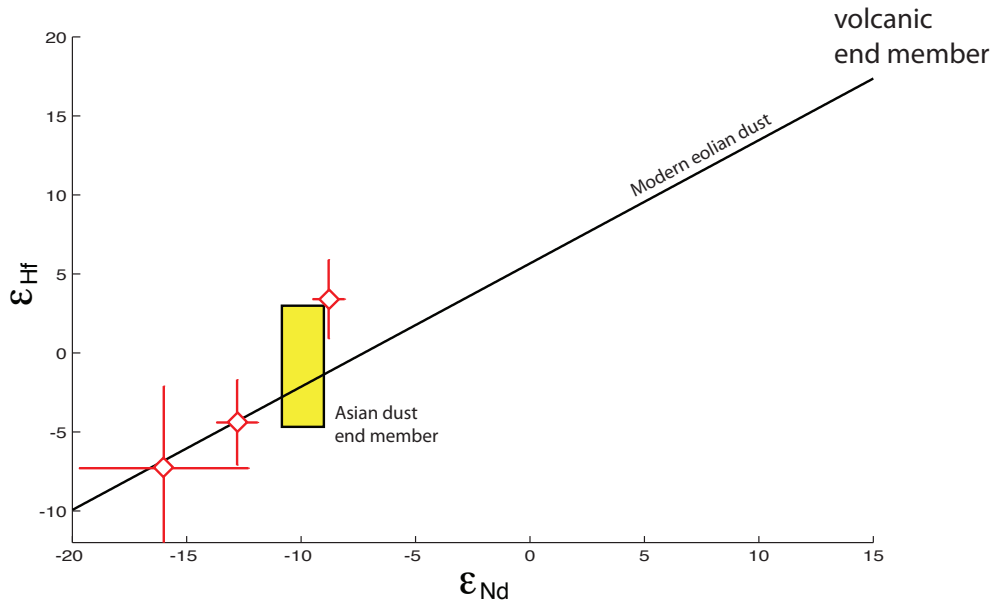


Figure 18: Neodymium and hafnium composition of Dye-3 dust and ice. Asian dust member and Nd-Hf correlation of modern aeolian dust are from Pettke *et al.* (2002).

excluded. Evidence for material transported from North America to Greenland has been found (Rousseau *et al.* (2006) and Donarummo *et al.* (2003)) but isotopic data is only available for limited parts of the source area. Contribution of other PSA dust to the dust deposited in Greenland is not unexpected. This additional PSA would add another mixing end member and would explain the observed differences between purely Asian dust and the dust composition found in Greenland. The isotopic characteristics of this additional source area has to have a lower  $^{87}\text{Sr}/^{86}\text{Sr}$  ratio and a lower  $\epsilon_{\text{Nd}}$  to be able to reproduce the observed values. This hypothesis is supported by our Hf isotopic data: two samples (132A and 132B) are less radiogenic than Asian dust which would indicate a potential mixing with another less radiogenic source area.

Given the three possible scenarios, mixing of Asian derived dust with another dust source is the best explanation for the observed dust composition in the Greenland Dye-3 ice core. In absence of more PSA information this source cannot yet be identified, but Saharan and Northern American dust are likely candidates.

## 4.2 Isotopic composition of the ice

The Nd and Sr isotopic composition of the dust free ice fraction shows variability in  $\epsilon_{Nd}$  whereas the  $^{87}Sr/^{86}Sr$  value is homogeneous. No study we are aware of has focused on pure ice composition on Greenland and little is known about Sr and Nd in precipitation (Herut *et al.* (1993); Negrel & Roy (1998); Nakano *et al.* (2006)) but either no attempt has been made to separate the dust fraction or water has not been buffered to avoid carbonates dissolution after collection. We speculate here that the origin of the measured Sr and Nd of the ice fraction can possibly be attributed to several sources: (1) leaching of carbonates and evaporite dissolution from the dust fraction during mobilization and transport, (2) oceanic derived Sr and Nd through seawater evaporation or sea spray, (3) windblown, sea ice derived, brine and salts.

The  $^{87}Sr/^{86}Sr$  is close to the constant sea water value (0.70916, (Palmer & Edmond, 1988)) and does not show large variations from sample to sample. Furthermore the measured uranium activity ratios ( $^{234}U/^{238}U$ ) of the water fraction (results not shown here, S. Aciego IGMR- ETHZ) strongly support a sea water origin of the ice fraction (activity of 1.1). These two isotopic systems are in agreement with recent model studies that show that more than 95% off the Greenland precipitation originates in the Atlantic or the Arctic ocean (Sodemann *et al.*, accepted). The leaching and mixing of dust during mobilization can therefore be rejected. Leaching of the carbonates and even dissolution of the evaporites during transport when "dusty" air masses mix with moist oceanic air is still a possibility. The Nd isotopic composition of the water is not obviously correlated to the isotopic composition of the dust extracted from the same ice core section (c.f. fig.17 - p. 49) but the small variations observed in the  $^{87}Sr/^{86}Sr$  ratios of the water fraction vary along with the corresponding  $^{87}Sr/^{86}Sr$  ratios of the dust fraction which could indicate a relationship between dust and ice. But considering the Sr/Nd ratio in PSA leachates that range between 20 and 75 (Honda *et al.*, 2004) and typical seawater Sr/Nd ratios of 4000 to 2000 (Palmer & Edmond (1988) and Lacan & Jeandel (2005)) the measured Sr/Nd ratios of our ice samples would have to be derived purely from dissolution which is in contradiction to the U activity ratios and the measured  $^{87}Sr/^{86}Sr$  of the ice fraction.

The measured Sr/Nd concentration ratios also indicate that the Sr and Nd measured in the ice cannot be directly derived from seawater evaporation because higher Sr/Nd ratios would be expected. Overall Sr and Nd concentrations in the ice would also be expected to be lower due to the distillation effect of the evaporation of oceanic water. Another marine related source is necessary to

account for the Sr and Nd concentrations measured. While little is known about sea spray salts and sea ice brine, they are possible candidates for the measured composition of the ice. Sea spray salts or sea ice brine could be formed and directly wind blown or transported to Greenland or re-dissolved by the precipitation and the liquid aerosols and induce favored concentration of Nd compared to Sr. If the isotopic composition is conserved during the aerosols formation, complementary information about the origin of the air masses leading to precipitation could be inferred and linked to the atmospheric circulation. Sodemann *et al.* (accepted), show that the origin of the winter Greenland precipitation is controlled by the Northern Atlantic Oscillation (pressure difference between the Icelandic low and Açores high that controls the weather regime of the northern hemisphere). We could then speculate that the isotopic Nd composition of the ice reflects the composition of the surface sea water at the evaporation site.

But in absence of further investigation of the processes affecting concentrations and isotopic composition during sea salt and brine formation, no definitive conclusion can be drawn regarding the origin of the Nd and Sr found in the ice. Nevertheless, the isotopic composition of dust free ice could be a valuable and promising tool for further climate reconstruction.

## 5 Conclusion

Previous ice core studies indicated that Asia is the primary source of the mineral dust transported to the Greenland ice sheet. But, concentrations of dust limited radiogenic isotopic measurements to dusty glacial ice, or to large-volume modern snow samples. The previous ice core studies did not show the variability observed in the high resolution snow-pit studies, likely due to the integration of the signal over hundreds of years. This work demonstrates the feasibility of high resolution dust isotopic measurements on small sample sizes, including the measurement of hafnium.

A new method was set up for the determination of the isotopic composition of strontium, neodymium and hafnium of the dust and ice fractions. The validation of the method, using certified rock standards and the regular verification of blank levels, assured the data quality and reliability. The results shown here indicate that it is possible to collect accurate isotopic data on small amounts of material: 5-10ng of Sr, 0.5-3ng of Nd, and 0.3-1ng of Hf. Furthermore, the precision of these measurements are high enough to resolve the large differences in isotopic composition of the dust source areas.

The significance of the resulting ice core dust record is twofold. First, given that the literature PSA isotopic data is representative of potential source areas, Asia is the main contributor to the dust content in the sections analyzed from the Dye-3 ice core. Variability within Asian sources is detected, with an alternating contribution of the Gobi and Taklimakan deserts and the Ordos plateau, consistent with previous studies. Second, differences in isotopic composition between known PSAs and dust samples suggests the existence of an additional dust source mixing with Asian dust in Greenland. Hf isotopic data shows that in our samples volcanic aerosols contribute only to a minor degree, if at all, to the dust load at Dye-3 and can not explain the observed differences. Sahara and North America are good candidates for the missing dust source but the current coverage of source areas is insufficient to capture the full range of potential source areas for the dust load in Greenland and more sampling is necessary.

There is further potential for investigating paleo-transport pathways by using the dust free ice fractions. The ice fraction carries a strong marine signature and the observed isotopic variations could be linked to different origins of water masses that lead to precipitation in Greenland. Nevertheless intermediate processes between the water mass and precipitation are necessary to explain the observed elemental concentrations and not enough is known to conclude to an origin of precipitation. We speculate here that sea ice or sea salts could have an important

role in these processes.

In the future, this method could be extended to different ice core locations and ages, thereby improving our understanding of the changing atmospheric dynamics through time.

## References

- Balcaen, L., DeSchrijver, I., Moens, L. & Vanhaecke, F. (2005). Determination of the  $^{87}\text{Sr}/^{86}\text{Sr}$  isotope ratio in USGS silicate reference materials by multi-collector icp-mass spectrometry. *Mass Spectrometry*, **242**, 251–255.
- Barnola, J., Raynaud, D., Korotkevich, Y. & Lorius, C. (1987). Vostok ice cores provides 160,000-year record of atmospheric CO<sub>2</sub>. *Nature*, **329**, 408–414.
- Birck, J. (1986). Precision K-Rb-Sr isotopic analysis: application to Rb-Sr chronology. *Chemical Geology*, **56**, 73–83.
- Biscaye, P. (1965). Mineralogy and sedimentation of recent deep-sea clay in atlantic ocean and adjacent seas and oceans. *Geological Society of America bulletin*, **76**, 803–831.
- Biscaye, P., Grousset, F., Revel, M., Van der Gaast, S., Zielinski, G., Vaars, A. & Kukla, G. (1997). Asian provenance of glacial dust (stage2) in the Greenland Ice Sheet Project 2 ice core, Summit, Greenland. *Journal of Geophysical Research*, **102**, 26765–26781.
- Bory, A., Biscaye, P., Svensson, A. & Grousset, F. (2002). Seasonal variability in the origin of recent atmospheric mineral dust at NorthGRIP, Greenland. *Earth and Planetary Science Letters*, **196**, 123–134.
- Bory, A., Biscaye, P., & Grousset, F. (2003a). Two distinct seasonal asian source regions for mineral dust deposited in Greenland (NorthGRIP). *Geophysical Research Letters*, **30**, 161–164.
- Bory, A., Biscaye, P., Piotrowski, A. & Steffensen, J. (2003b). Regional variability of ice core dust composition and provenance in greenland. *Geochemistry, Geophysics and Geosystems*, **4**.
- Burton, G., Rosman, K., Candelone, J., Burn, L., Boutron, C. & Hong, S. (2007). The impact of climatic conditions on pb and sr isotopic ratios found in Greenland ice, 7-150 kyr BP. *Earth and Planetary Science Letters*, **259**, 557–566.
- Capo, R., Stewart, B. & Chadwick, O. (1998). Strontium isotopes as tracers of ecosystem processes: theory methods. *Geoderma*, **82**, 197–225.
- Caro, G., Bourdon, B., Birck, J. & Moorbath, S. (2006). High-precision  $^{142}\text{Nd}/^{144}\text{Nd}$  measurements in terrestrial rocks: Constraints on the early differentiation of the earths mantle. *Geochimica et Cosmochimica Acta*, **70**, 164–191.

- Chappelaz, J., Barnola, J., Raynaud, D., Korotkevich, Y. & Lorius, C. (1990). Ice-core record of atmospheric methane over the past 160,000 years. *Nature*, 127–131.
- Chen, J., Li, G., Yang, J., Rao, W., Lu, H., Balsam, W., Sun, Y. & Ji, J. (2007). Nd and Sr isotopic characteristics of chinese deserts: implication for provenance of asian dust. *Geochimica et Cosmochimica Acta*, **71**, 3904–3914.
- Chester, R. & Johnson, L. (1971). Trace element geochemistry of the North aeolian dusts. *Marine Geology*, **231**, 176–178.
- Clausen, H., Hammer, C., Hvidberg, C., Dahl-Jensen, D., Steffensen, J., Kipfstuhl, J. & Legrand, M. (1997). A comparison of the volcanic records over the past 4000 years from the Greenland Ice Core Project and Dye 3 Greenland ice cores. *Journal of Geophysical Research*, **102**, 26707–26723.
- Connelly, J., Ulfbeck, D., Thrane, K., Bizzarro, M. & Housh, T. (2006). A method for purifying lu and h for analyses by MC-ICP-MS using TODGA resin. *Chemical Geology*, **233**, 126–136.
- Dansgaard, W., Clausen, H., Gundestrup, N., C.U., H., Johnsen, S., Kristinsdottir, P. & Reeh, N. (1982). A new Greenland deep ice core. *Science*, **218**, 1273–1277.
- Dasch, E. (1969). Strontium isotopes in weathering profiles, deep-sea sediments and sedimentary rocks. *Geochimica et Cosmochimica Acta*, **33**, 1521–1552.
- DePaolo, W. & Wasserburg, G. (1976). Nd isotopic variations and petrogenetic models. *Geophysical research letters*, **3**, 249–252.
- Derry, L. & France-Lanord, C. (1996). Neogene himalayan weathering history and river 87Sr/86Sr: impact on the marine Sr record. *Earth and Planetary Science Letters*, **3**, 59–74.
- Donarummo, J., Ram, M. & E.F., S. (2003). Possible deposit of soil dst from the 1930's u.s. dust bowl identified in greenland ice. *Geophysical Research Letters*, **30**.
- Dymond, J., Biscaye, P. & Rex, R. (1974). Eolian origin of mica in hawaiian soils. *Geological Society of America Bulletin*, **85**, 37–40.
- Gallet, S., Jahn, B. & Torii, M. (1996). Geochemical characterization of the luochuan loess-paleosol sequence, China, and paleoclimatic implications. *Chemical Geology*, **133**, 67–88.

- Gerstenberger, H. & Haase, G. (1997). A highly effective emitter substance for mass spectrometric Pb isotope ratio determinations. *Chemical Geology*, **136**, 309–312.
- Goldstein, S. & Stirling, C. (2003). *Techniques for measuring Uranium-series nuclides: 1992 - 2002.*, vol. 52. Reviews in Mineralogy and Geochemistry - Uranium-Series Geochemistry, B. Bourdon, G.M. Henderson and C.C. Lundstrom and S.P. Turner - Mineralogical Society of America.
- Grootes, P., Stuiver, M., White, J., Johnsen, S. & Jouzel, J. (1993). Comparison of oxygen isotope records from the GISP2 and GRIP Greenland ice cores. *Nature*, **366**, 552–554.
- Grousset, F. & Biscaye, P. (2005). Tracing dust sources and transport patterns using sr, nd and pb isotopes. *Chemical Geology*, **222**, 149–167.
- Hamilton, W. & Langway, C. (1967). A correlation of microparticle concentrations with oxygen isotope ratios in 700 year old Greenland ice. *Earth and Planetary Science Letters*, **3**, 363–366.
- Hammer, C., Clausen, H., Dansgaard, W., Neftel, A., Kristinsdottir, P. & Johnson, E. (1985). *Continuous imurity analysis along the Dye-3 deep core*, in, vol. Geophysical Monograph 33. American Geophysical Union, Washington DC.
- Hanyu, T., Nakai, S. & Tatsuta, R. (2005). Hafnium isotope ratios of nine GSJ reference samples. *Geochemical Journal*, **39**, 83–90.
- Herut, B., Starinsky, A. & Amitai, K. (1993). Strontium in rainwater from Israel: sources, isotopes and chemistry. *Earth and Planetary Science Letters*, **120**, 77–84.
- Honda, M., Yabuki, S. & Shimizu, H. (2004). Geochemichal and isotopic studies of aeolian sediments in china. *Sedimentology*, **51**, 211–230.
- Horwitz, E., Chiarizia, R. & Dietz, M. (1992). A novel strontium-selective extraction chromatographic resin. *Solvent Extraction and Ion Exchange*, **10**, 313–342.
- IPCC AR4 (2007). *Climate change 2007 the physical science basis - Contribution of working group I to the Fourth Assesment Report of the Intergovernmental Panel on Climate Change.*. Cambridge University press.
- Jones, C., Halliday, A., Rea, D. & Owen, R. (1994). Neodymium isotopic variations in North Pacific modern silicate sediment and the insignificance of detrital ree contributions to seawater. *Earth and Planetary Science Letters*, **127**, 55–66.

- Jones, C., Halliday, A., Rea, D. & Owen, R. (2000). Eolian inputs of lead to the North Pacific. *Geochimica et Cosmochimica Acta*, **64**, 1405–1416.
- Kanayama, S., Yabuki, S., Yanagisawa, F. & Motoyama, R. (2002). The chemical and strontium isotope composition of atmospheric aerosols over Japan: the contribution of long-range-transported Asian dust (kosa).. *Atmospheric Environment*, **36**, 5159–5175.
- Kanayama, S., Yabuki, S., Zeng, F., Liu, M., Shen, Z., Liu, L., Yanagisawa, F. & Abe, O. (2005). Size-dependant geochemical characteristics of Asian dust, Sr and Nd isotope compositions as tracers for source identification. *Journal of the meteorological society of Japan*, **83A**, 107–120.
- Korkisch, J. (1988). *Handbook of Ion Exchange Resins: Their Application to Inorganic Analytical Chemistry*.. CRC Press.
- Lacan, F. & Jeandel, C. (2005). Neodymium isotopes as a new tool for quantifying exchange fluxes at the continent-ocean interface. *Earth and Planetary Science Letters*, **3-4**, 245–257.
- Langway, C., Oeschger, H. & Dansgaard, W. (1985). *The Greenland ice sheet program in perspective*, in, vol. Geophysical Monograph 33. American Geophysical Union, Washington DC.
- LeFevre, B. & Pin, C. (2001). An extraction chromatography method for Hf separation prior to isotopic analysis using multiple collection ICP-mass spectrometry. *Analytical Chemistry*, **73**, 2453–2460.
- Martin, J. (1991). Iron still comes from above. *Nature*, **353**.
- Münker, C., Weyer, S., Scherer, E. & Mezger, K. (2001). Separation of high field strength elements (Nd, Ta, Zr, Hf) and Lu from rock samples for MC-ICPMS measurements. *Geochemistry Geophysics Geosystems*, **2**.
- Nakano, T., Morohashi, S., Yasuda, H., Sakai, M., Aizawa, S., Shichi, K., Morisawa, T., Takahashi, M., Sanada, M., Matsuura, Y., Sakai, H., Akama, A. & Okada, N. (2006). Determination of seasonal and regional variation in the provenance of the dissolved cations in rain in Japan based on Sr and Pb isotopes. *Atmospheric Environment*, **40**, 7409–7420.
- Negrel, P. & Roy, S. (1998). Chemistry of rainwater in the Massif Central (France): a strontium isotope and major element study. *Applied Geochemistry*, **13**, 941–951.
- NuInstruments (1998). *Nu Plasma Operating Manual*.

- Palmer, M. & Edmond, J. (1988). The strontium isotope budget of the modern ocean. *Earth and Planetary Science Letters*, **92**, 11–26.
- Patchett, P. (1983). Importance of the Lu-Hf isotopic system in studies of planetary chronology and chemical evolution. *Geochemica et Cosmochimica Acta*, **47**, 81–91.
- Petit, J.R., Jouzel, J., Raynaud, D., Barkov, N.I., Barnola, J.M., Basile, I., Bender, M., Chappellaz, J., Davis, M., Delaygue, G., Delmotte, M., Kotlyakov, V.M., Legrand, M., Lipenkov, V.Y., Lorius, C., Pepin, L., Ritz, C., Saltzman, E. & Stievenard, M. (1999). Climate and atmospheric history of the past 420,000 years from the vostok ice core, antarctica. *Nature*, **399**, 429–436.
- Pettke, T., Der-Chuen, L., Halliday, A. & Rea, D. (2002). Radiogenic hf isotopic compositions of continental aeolian dust from asia, its variability and its implications for sea water hf. *Earth and Planetary Science Letters*, **202**, 453–464.
- Pin, C. & Zalduegui, J. (1994). Concomitant separation of strontium and samarium-neodymium for isotopic analysis in silicate samples, based on specific extraction chromatography. *Analytica Chimica Acta*, **298**, 209–217.
- Potts, P. (1987). *A handbook of silicate rock analysis*. Chapman and Hall.
- Prospero, J., Glaccum, R. & Nees, R. (1981). Atmospheric transport of soil dust from Africa to South America. *Nature*, **289**, 570–573.
- Prospero, J., Ginoux, P., Torres, O., Nicholson, S. & Gill, T. (2002). Environmental characterization of global sources of atmospheric soil dust indentified with the NIMBUS 7 total ozone mapping spectrometer (toms) absorbing aerosol product. *Reviews of Geophysics*, **40-1**.
- Raczek, I., Jochum, P. & Hofmann, W. (2003). Neodymium and strontium isotop data for USGS reference materials BCR-1, BCR-2, BHVO-1, BHVO-2, AGV-1, AGV-2, GSP-1, GSP-2 and eight MPI-DING glasses. *Geostandards*, **27**, 173–179.
- Raisbeck, G., Yiou, F., Bourles, D., Lorius, C., Jouzel, J. & Barkov, N. (1987). Evidence for 2 intervals of enhanced Be-10 deposition in antarctic ice during the last glacial period. *Nature*, **326**, 273–277.
- Ram, M. & Koenig, G. (1997). Continuous dust concentration profile of pre-Holocene ice from the Greenland Ice Sheet Project 2 ice core: dust stadials, interstadials, and the Eemian. *Journal of Geophysical Research*, **102**, 26641–26648.

- Rao, W., Yang, J. & Li, G. (2006). Sr-Nd isotope geochemistry of eolian dust of the arid-semiarid areas in China: Implications for loess provenance and monsoon evolution. *Chinese Science Bulletin*, **51**, 1401–1412.
- Raymo, M. & W.F., R. (1992). Tectonic forcing of late cenozoic climate. *Nature*, **359**, 117–122.
- Rea, D. (1994). The paleoclimatic record provided by eolian deposition in the deep sea: the geological history of wind. *Reviews of Geophysics*, **32**, 159–195.
- Rehkämper, M., Schönbächler, M. & Stirling, C.H. (2001). Multiple collector ICP-MS: Introduction to instrumentation, measurement techniques and analytical capabilities. *Geostandards*, **25**, 23–40.
- Rousseau, D., Schevin, P., Duzer, D., Cambon, G., Ferrier, J. & Jolly, D. (2006). New evidence of long distance pollen transport to southern Greenland in late spring. *Review of Paleobotany and Palynology*, **141**, 277–286.
- Ruth, U., Wagenbach, D., Steffensen, J. & Bigler, M. (2003). Continuous record of microparticle concentration and size distribution in the central Greenland NGRIP ice core during last glacial period. *Journal of Geophysical Research*, **108**.
- Sarnthein, M., Tetzlaff, G., Koopmann, B., Wolter, K. & Pflaumann, U. (1981). Glacial and interglacial wind regimes over the eastern subtropical Atlantic and North-West Africa. *Nature*, **293**, 193–196.
- Schi, Z., Shao, L., Jones, T. & Lu, S. (2005). Microscopy and mineralogy of airborne particles collected during severe dust storm episodes. *Journal of Geophysical Research*, **110**.
- Schulz, M., Balkanski, Y., Guelle, W. & Dulac, F. (1998). Role of aerosol size distribution and source location in a three dimensional simulation of a saharan dust episode tested against satellite-derived optical thickness. *Journal of Geophysical Research*, **103**, 10579–10592.
- Schutz, L. & Seibert, M. (1987). Mineral aerosols and source identification. *Journal of Aerosol Science*, **18**, 1–10.
- Shirahata, H., Elias, R., Patterson, C. & Koide, M. (1980). Chronological variations in concentrations and isotopic composition of anthropogenic atmospheric lead in sediments of a remote subalpine pond. *Geochimica et Cosmochimica acta*, **44**, 149–162.

- Sigg, A. (1990). *Wasserstoffperoxide-Messungen an Eisbohrkernen aus Gronland und der Antarktis und ihre atmospharenchemische Bedeutung*. Ph.D. thesis, Philosophisch-naturwissenschaftlichen Fakultat der Universitat Bern.
- Sodemann, M., Schwierz, C. & Wernli, H. (accepted). Inter-annual variability of greenland winter precipitation source. part i: Lagrangian moisture diagnostic and north atlantic oscillation influence. *Journal of Geophysical research*.
- Steffensen, J. (1997). The size distribution of microparticles from selected segments of the Greenland Ice Core Project ice core representing different climatic periods. *Journal of Geophysical Research*, **102**, 26755–26763.
- Stukas, V. & Wong, C. (1981). Stable lead isotopes as a tracer in coastal waters. *Science*, **211**, 1424–1427.
- Sullivan, R., Guazzotti, S., Sodeman, D. & Prather, K. (2006). Direct observation of atmospheric processing of asian mineral dust. *Atmos. Chem. Phys. Discuss.*, **211**, 4109–4170.
- Svensson, A., Biscaye, P. & Grousset, F. (2000). Characterization of late glacial continental dust in the Greenland Ice Core Project ice core. *Journal of Geophysical Research*, **105**, 4637–4656.
- Tanaka, T. & Chiba, M. (2006). A numerical study of the contributions of the dust source regions to the global dust budget. *Global and Planetary Change*, **52**, 88–104.
- Tanaka, T., Togashi, S., Kamioka, H., Amakawa, H., Kagami, H., Hamamoto, T., Yuhara, M., Orihashi, Y., Yoneda, S., Shimizu, H., Kunimaru, T., Takahashi, K., Yanagi, T., Nakano, T., Fujimaki, H., Shinjo, R., Asahara, Y., Tanimizou, M. & Dragusanu, C. (2000). Jndi-1: a neodymium isotopic reference in consistency with lajolla neodymium. *Chemical Geology*, **168**, 279–281.
- ThermoFinnigan (2002). *Triton Hardware Manual*.
- Thomas, R. (2001). Spectroscopy tutorial - a beginner's guide to ICP-MS. *Spectroscopy*, **16-17**.
- Vajda, N., LaRosa, J., Danesi, P. & Kis-Benedek, G. (1997). A novel technique for simultaneous determination of  $^{210}\text{Pb}$  and  $^{210}\text{Po}$  using a crown ether. *Journal of Environmental Radioactivity*, **37**, 355–372.
- Vinther, B., Clausen, H., Johnson, S., Rasmussen, S., Andersen, K., Buchardt, S., Dahl-Jensen, D., Seierstad, I., Siggard-Andersen, M., Steffensen, J., Svensson,

- A. & Heinemeier, J. (2006). A synchronized dating of three greenland ice-cores throughout the holocene. *Journal of Geophysical Research*, **111**.
- Waight, T., Baker, J. & Peate, D. (2002). Sr isotope ratio measurements by double-focusing MC-ICPMS: techniques, observations and pitfalls. *International Journal of Mass Spectrometry*, **221**, 229–244.
- Weis, D., Kieffer, B., Hanano, D., Nobre Silva, I., Barling, J. & Pretorius, W. (2007). Hf isotope compositions of U.S. Geological Survey reference materials. *Geochemistry, Geophysics, Geosystems*, **8**.
- White, W., Patchett, J. & BenOthman, D. (1986). Hf isotope ratios of marine sediments and Mn nodules: evidence for a mantle source of Hf in seawater. *Earth and Planetary Science Letters*, **79**, 46–54.
- Xiao, J., Inouchi, Y., Kumai, H., Yoshikawa, S., Kondo, Y., Liu, T. & An, Z. (1996). Dust: A diagnostic of the hydrologic cycle during the Last Glacial Maximum. *Science*, **271**, 962–963.
- Yokoo, Y., Nakano, T., Nishikawa, M. & Quan, H. (2004). Mineralogical variation of Sr-Nd isotopic and elemental compositions in loess and desert sand from the central loess plateau in china as a provenance tracer for wet and dry deposition in the northwestern Pacific. *Chemical Geology*, **204**, 45–62.
- Zdanowicz, C., Hall, G., Vaive, J., Amelin, Y., Percival, J., Girard, I., Biscaye, P. & Bory, A. (2006). Asian dustfall in the St. Elias Mountains, Yukon, Canada. *Geochimica et Cosmochimica Acta*, **70**, 3493–3507.

# APPENDIX

## A Lead: methods, results and pitfalls

The analysis of lead (Pb) isotopic composition of the dust was intended to be carried out during this work. Pb isotopes, in combination to Sr, Nd and Hf was expected to contribute greatly to the definition of potential source areas of the dust found in the Greenland ice. Several studies have shown that the Pb isotopic composition of dust samples varies from location to location, and can be used to discriminate PSAs (Biscaye *et al.* (1997); Jones *et al.* (2000); Grousset & Biscaye (2005); Burton *et al.* (2007)).

We present here the work that has been done during this study on Pb isotopic measurements, and discuss the possible reasons for the unsuccessful results on the Greenland dust samples.

**Isotopes** Lead - Pb is a metal with atomic number 82. It is relatively abundant and has 4 natural isotopes.  $^{204}\text{Pb}$  is radiogenic and decays to  $^{200}\text{Hg}$  by emission of an  $\alpha$ -particle with a half life of  $1.4 \times 10^{17}$  years.  $^{206}\text{Pb}$ ,  $^{207}\text{Pb}$  and  $^{208}\text{Pb}$  are stable isotopes produced respectively from the decay of  $^{238}\text{U}$ ,  $^{235}\text{U}$  and  $^{232}\text{Th}$  through a decay chain involving several radionuclides.  $^{210}\text{Pb}$  is short lived (22.4 years) and decays to  $^{206}\text{Pb}$  by  $\alpha$ -decay and  $^{210}\text{Bi}$  by  $\beta$ -decay.

Isotope	$^{204}\text{Pb}$	$^{206}\text{Pb}$	$^{207}\text{Pb}$	$^{208}\text{Pb}$	$^{210}\text{Pb}$
Abundance	0.0014	0.0241	0.221	0.524	<i>traces</i>

Table 18: Lead isotopes natural abundances.

The simultaneous decay of two U isotopes to two Pb isotopes has been widely used for dating purposes by studying  $^{207}\text{Pb}/^{204}\text{Pb}$  and  $^{206}\text{Pb}/^{204}\text{Pb}$  systems. Lead has also been applied as a tracer for natural processus (e.g. Stukas & Wong, 1981) and environmental studies (e.g. Shirahata *et al.*, 1980).

**Mass spectrometry** Pb isotopes were measured on TIMS (c.f. 2.1.3 - p.19) for accurate measurement of small samples.

**Loading** The lead collected off the Sr-spec column was dried down on a hot plate and, before reaching complete dryness, a small drop of 0.25N phosphoric acid added. Pb was then loaded onto single Re filaments, that were acid cleaned and carefully outgassed before use (2 hours at 4.5A), along with an equivalent amount of silica gel activator (Gerstenberger & Haase, 1997). The 1 to 2  $\mu\text{l}$  solution was dried down on the filament at  $\sim 0.5\text{A}$ . The filament current was then

increased slowly to let the phosphoric acid evaporate before heating up to dull red.

### Cup configuration

Farraday cup	L1	C	H1	H2	H3
Pb isotope	$^{204}\text{Pb}$	$^{205}\text{Pb}$	$^{206}\text{Pb}$	$^{207}\text{Pb}$	$^{208}\text{Pb}$

Table 19: Cup configuration for Pb analysis.

**Measurement procedure** Certified standard solution and rock standards were measured following the same procedure. After performing a baseline of 150s, the filament was heated up to 1300°C at 200°C/min and after focusing the ion beam the measurement was started without any further change to the filaments' current. Once the first measurement finished, a second was carried out at 1350°C after re-focusing, and a third at 1450°C after focusing. Several other temperatures stages were tested over the measurement period, but heating rates were kept identical.

Measurements	Integration time	Blocks	Cycles	Inter-block actions
200	4sec	10	20	None

Table 20: Measurement procedure for Pb

**Standard results - NBS981 and mass fractionation** Unlike Sr, Nd and Hf, lead has only one isotope that is not the product of radioactive decay making the use of internal mass fractionation correction impossible. The method chosen is to correct measured sample ratios by external mass fractionation correction (c.f. 2.4.1 - p.28). The  $\beta$  value is calculated by applying the power law (c.f. eq. 2 - p.28) to the certified standard solutions measurements. To be valid, this method needed to achieve a high reproducibility amongst the certified standard solution runs, meaning that the loading and the measurement conditions must be similar from measurement to measurement. Certified solutions of various loads have been measured over different temperature ranges according to the measurement procedure described in the previous paragraph. These measurements were used to calculate mass fractionation factors at different temperatures.

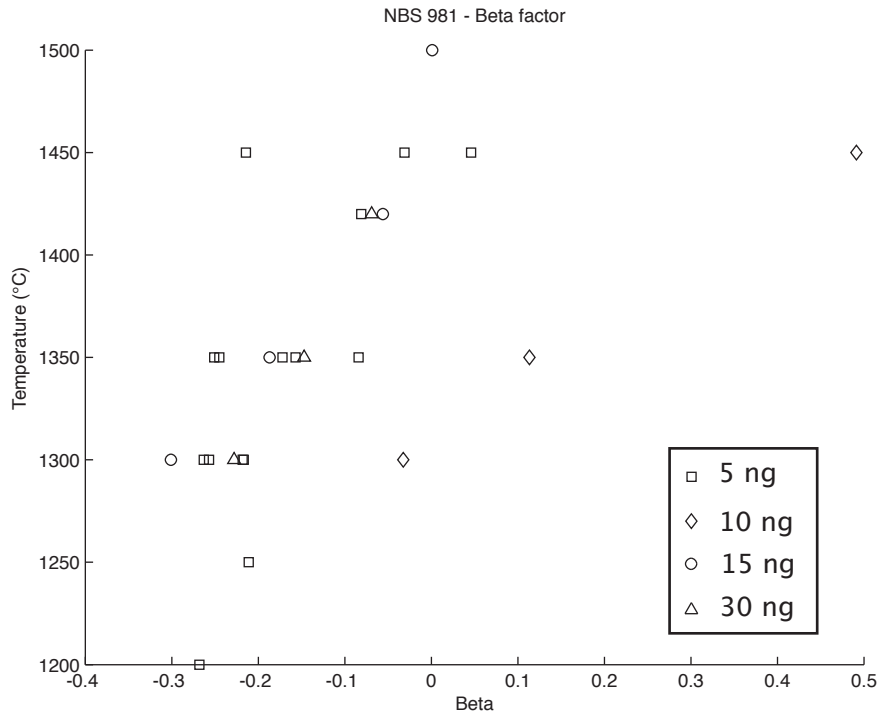


Figure 19:  $\beta$  factor calculated from NBS981 measurements.

Based on the NBS981 measurements, we decided that measurements carried out at 1300°C were the most reliable and reproducible in terms of  $\beta$  factors, involving high enough beam intensity for an accurate measurement as well as consistent correction factors from run to run with small sample size dependency.

**Pitfalls** BCR-2 rock standards were measured and corrected for mass fractionation using the external mass fractionation correction based on NBS9181 measurements. The results were not completely satisfactory. The external mass fractionation correction necessitates a high reproductivity for both standard and sample measurements and in our case it was often observed that the ionization initiation temperature was changing from run to run. In some cases, ionization seemed not to take place at all or was not detected. This could possibly be due to the silicagel activator solution used to increase ionization efficiency. This activator could polymerize and then inhibit ionization.

This also leads to the reflection about the measurement procedure itself. By using a single starting temperature for measurement of sample and standard, the risk is high that for small samples valuable material has already evaporated off the fila-

ment before the measurement starts. In the absence of double spike availability, total evaporation measurement modes could be interesting to remove this issue eventhough other problems may arise.

## B Column elution procedures

<b>Tru-spec column - All elements</b>		
Column volume : 500 $\mu$ l		Resin mesh : 50-100 $\mu$ m
Duration $\sim$ 4 hours		
Cleaning	2ml 3ml 2ml 2ml	MQ $H_2O$ 10N $HCl$ 1N $HCl$ 0.1N $HCl$ - 1N $HF$
Condition	1ml 1ml 1ml	MQ $H_2O$ 1N $HCl$ 10N $HCl$
Load and collect Ra - Sr - Pb	1ml	10N $HCl$ - Boric ac.
Collect Ra - Sr - Pb	0.75ml	10N $HCl$
Collect HFSE, REE	0.25ml 2.5ml	1N $HCl$ 1N $HCl$
Collect U - Pa	2.5ml	0.1N $HCl$ - 1N $HF$

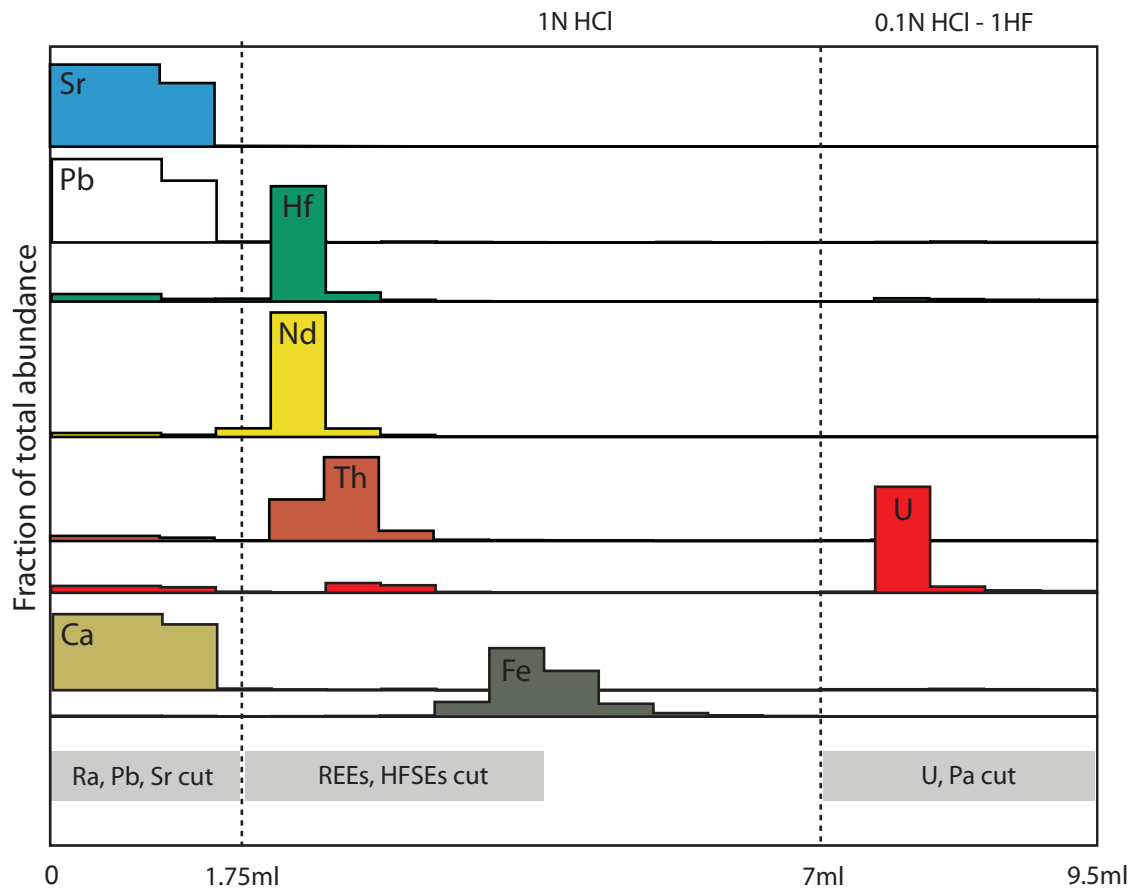


Figure 20: Elution curve obtained from the Truspec column using the BCR-2 rock standard.

<b>Sr-spec column - Ra, Sr, Pb separation</b>		
Column volume : 100 $\mu\text{l}$		Resin mesh : 50-100 $\mu\text{m}$
Duration $\sim$ 4 hours		
Cleaning	3ml 3ml 3ml 3ml	3N $HNO_3$ MQ $H_2O$ 6N $HCl$ MQ $H_2O$
Condition	1ml	3N $HNO_3$
Load and Collect Ra	0.2ml	3N $HNO_3$
Collect Ra	0.3ml	3N $HNO_3$
Rinse Ba	3 x 0.5ml	7.5N $HNO_3$
Collect Sr	2 x 0.5ml	0.05N $HNO_3$
Change acides	0.1ml	MQ $H_2O$
Collect Pb	2 x 1ml	6N $HCl$

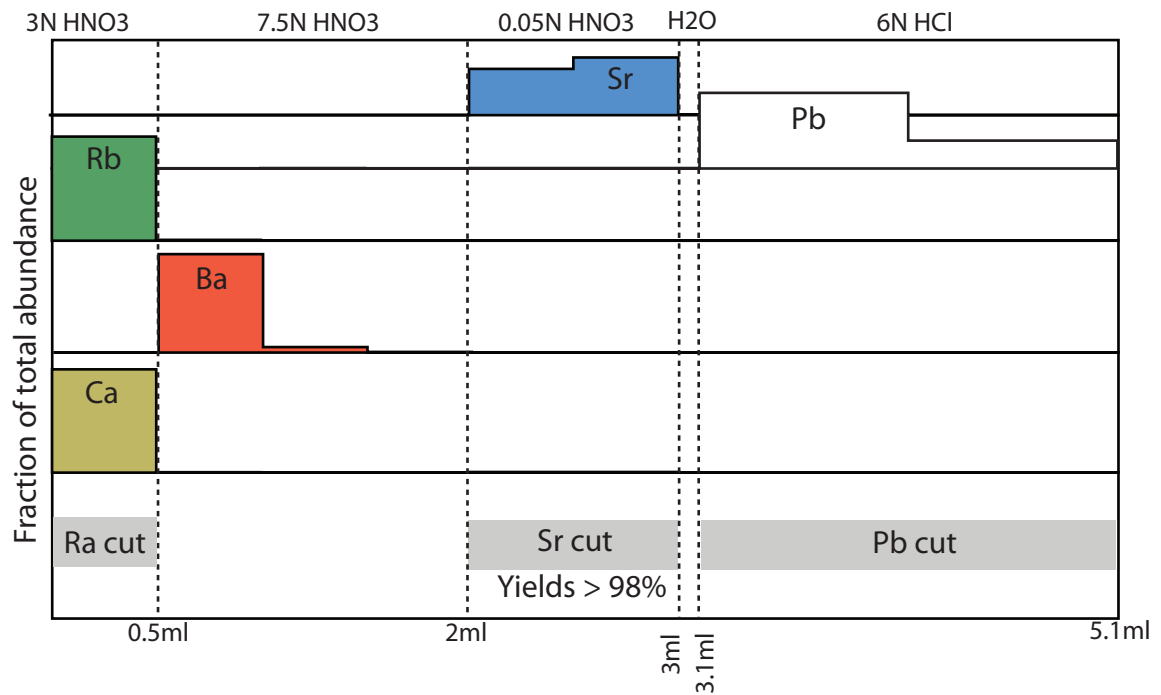


Figure 21: Elution curve obtained from the Srspec column using the BCR-2 rock standard.

<b>Ln-spec column - REEs, Th and Hf separation</b>		
Column volume : 700 $\mu$ l		Resin mesh : 50-100 $\mu$ m
Duration $\sim$ 12-13 hours		
Cleaning	5ml 5ml 5ml 5ml	6N <i>HCl</i> 2N <i>HF</i> 6N <i>HCl</i> 2N <i>HF</i>
Condition	6ml	1.2N <i>HCl</i>
Load and collect REEs	2.75ml	1.2N <i>HCl</i>
Collect REEs	0.7ml	3N <i>HCl</i>
Rinse Yb - Lu	8ml 8ml	6N <i>HCl</i> 3N <i>HCl</i>
Change acids	2 x 0.5ml	MQ <i>H<sub>2</sub>O</i>
Rinse Ti	5ml	0.09N Cit - 0.4N <i>HNO<sub>3</sub></i> - 1 wt% <i>H<sub>2</sub>O<sub>2</sub></i>
Rinse <i>H<sub>2</sub>O<sub>2</sub></i>	2ml	MQ <i>H<sub>2</sub>O</i>
Collect Th	3ml	3N <i>HCl</i> - 0.1N <i>HF</i>
Rinse Zr	2ml	3N <i>HCl</i> - 0.1N <i>HF</i>
Collect Hf	6ml	6N <i>HCl</i> - 0.3N <i>HF</i>

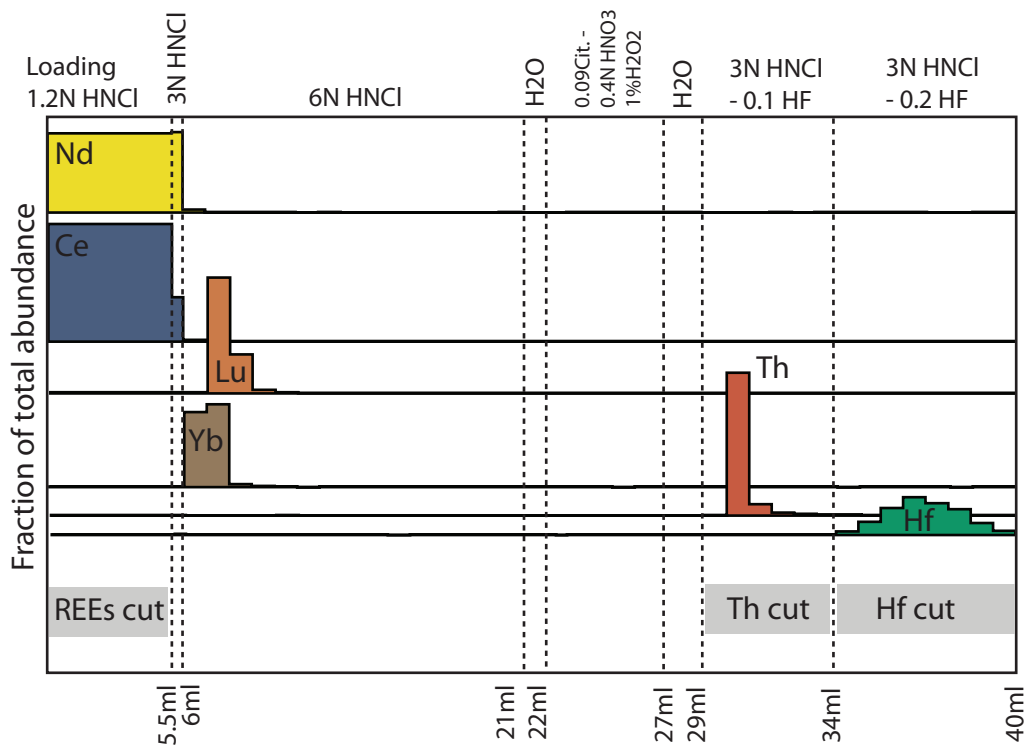


Figure 22: Earlier elution curve obtained from the Lnspec column using the BCR-2 rock standard. This column was further calibrated and final Hf yields were over 96 %.

<b>Ln-spec column - Sm, Nd separation</b>						
Column volume : 2000 $\mu$ l				Resin mesh : 50-100 $\mu$ m		
Duration ~8-10 hours						
	A	B	C	D	E	
Cleaning	4ml 2ml 4ml 2ml					1.2N <i>HCl</i> MQ <i>H<sub>2</sub>O</i> 1.2N <i>HCl</i> MQ <i>H<sub>2</sub>O</i>
Condition	2ml					0.25N <i>HCl</i>
Load	0.5ml					0.05N <i>HNO<sub>3</sub></i>
Rinse La, Ce, Pr	5ml	5.25ml	5.5ml	5.5ml	5.5ml	0.25N <i>HCl</i>
Collect Nd	3ml					0.3N <i>HCl</i>
Collect - Rinse Sm	3ml					1.2N <i>HCl</i>

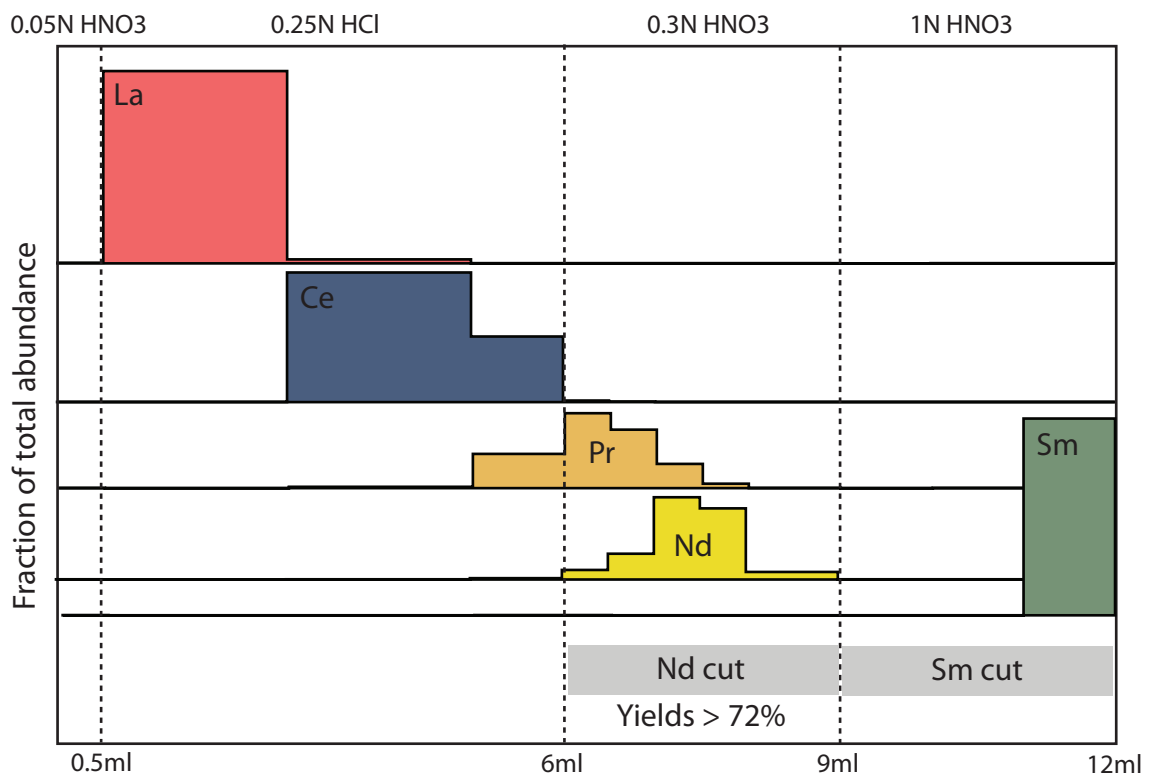


Figure 23: Elution curve obtained from the Lnspec REEs separation column using the BCR-2 rock standard.

## C Measuring U-Series Isotopes in Polar Ice

Measuring U-Series Isotopes in Polar Ice: Toward an Absolute Ice Chronometer, *Eos Trans. AGU*, 88(52), Fall Meet. Suppl., Abstract C15A-0108.

**Aciego, S M** - aciego@erdw.ethz.ch - Institute for Isotope Geochemistry and Mineral Resources, ETH-Zurich Clausiusstrasse 25, NW C83.1, Zurich, 8092, Switzerland.

**Bourdon, B** - bourdon@erdw.ethz.ch - Institute for Isotope Geochemistry and Mineral Resources, ETH-Zurich Clausiusstrasse 25, NW C83.1, Zurich, 8092, Switzerland.

**Schwander, J** - schwander@climate.unibe.ch - Climate and Environmental Physics, University of Bern Sidlerstrasse 5, Bern, 3012, Switzerland.

**Stocker, T** - stocker@climate.unibe.ch - Climate and Environmental Physics, University of Bern Sidlerstrasse 5, Bern, 3012, Switzerland.

Comparison of ice records between ice sheets, alpine glaciers, and marine records currently rely on a combination of ice layer counting, matching relative time scales, and interpolation. U-series recoil from mineral aerosols (dust) into the ice matrix is one possible technique for determining the absolute age of ice, independent of any other parameters. However, the low concentrations of the U-series parents and daughters have made previous measurements difficult and the results ambiguous. We present here the first results of work we have undertaken for determining U-series recoil ages in ice cores. The primary difficulty of this technique is the extremely low concentrations of dust in polar ice samples, and therefore, of the recoil daughter products in the ice. Previous work on dust provenance indicates 0.01 to 1 mg of dust concentration per kilogram of ice from the ice cores of Greenland and Antarctica. Given these conditions, U and Th dissolved in the water fraction of the aerosol-ice system may overwhelm the total U-series budget. Constraining the possible "initial" U and Th is the first step in determining the feasibility of this dating method for ice cores. We have implemented new geochemical techniques: ultra-clean ice processing, multiple ion counter ICP-MS measurements of U and Th, and quantification of total recoveries of the aerosol and water fractions using both established USGS standards, an internal lab loess standard that best approximates the dust fraction found in ice cores, and [U]-[Th] standards SRM960 and Th105. Dissolution experiments using U and Th spikes with these standards indicate recovery of the dust and dissolved fractions are better than 99%. We present here the first concentration measurements of U from the water fraction (inf. 0.2 microns) of freshly deposited South Pole snow (20pg/kg), as well as a series of measurements from the upper section (128m) of the Dye 3 ice core in Greenland which thus far range from 410pg/kg to 520fg/kg U dissolved

in the water fraction. The high  $^{234}\text{U}/^{238}\text{U}$  activity ratio (sup. 1) in the Greenland ice core indicates the source of the uranium within the dissolved fraction is not inconsistent with seaspray. Given these results we model, using a simple Monte Carlo simulation, the expected errors in measuring absolute ages of polar ice. Using an estimate of surface roughness factor of 160 (based on recent BET measurements of dust), a lognormal distribution of grain sizes around 2 microns, and concentrations of dust over glacial periods on the order of 0.5mg/kg, we find that our current blanks, detection limits and internal precision should allow us to measure the ages of polar ice with an accuracy of 1% for Antarctic Ice cores and 5-10% for Greenland Ice cores (2 sigma).